





RESEARCH ARTICLE

[View Article Online](#)
[View Journal](#)

Cite this: DOI: 10.1039/d5md00332f

Design, synthesis, molecular modeling, and antiproliferative evaluation of new 2-oxoindolin-3-ylidene thiazole derivatives†

Aalaa F. El-Mokadem, ^a Mohammed K. Abd El-Gaber, ^{*ab} Pak Hei Chung,^c Siang-Boon Koh, ^{cd} Hoda Y. Hassan^a and Adel F. Youssef ^{*a}

A series of novel 2-oxoindolin-3-ylidene thiazole derivatives were designed and synthesized, inspired by the pharmacophoric features of the VEGFR-2 inhibitor sunitinib. These compounds were evaluated for antiproliferative activity against a panel of sixty cancer cell lines at the US National Cancer Institute, identifying derivatives **4b**, **4c**, **4d**, **4l**, and **6c** as the most potent, with mean growth inhibition percentages of 118.86%, 135.32%, 148.27%, 126.16%, and 78.46%, respectively. Further cytotoxicity assessments against the HepG2 cell line revealed IC₅₀ values ranging from 3.13 to 30.54 μM. These compounds also demonstrated strong VEGFR-2 inhibition, with IC₅₀ values of 0.113, 0.047, 1.549, 0.995, and 0.089 μM, respectively, compared to sunitinib's IC₅₀ of 0.167 μM. Selectivity index analysis indicated high selectivity for HepG2 cells over THLE-2 normal cells (1.80–10.26), suggesting favourable safety profiles compared to sunitinib (1.15). Notably, compound **4c** induced G0/G1 phase cell cycle arrest, promoted apoptosis, upregulated caspase-3 and -9 expression, and delayed wound closure by 60.74%. Molecular docking studies confirmed strong binding interactions within the VEGFR-2 active site, while *in silico* ADME and DFT analyses supported favourable pharmacokinetic properties and reactivity. These findings position compound **4c** as a promising lead for the development of anticancer agents.

Received 16th April 2025,
Accepted 14th May 2025

DOI: 10.1039/d5md00332f

rsc.li/medchem

1. Introduction

Cancer remains one of the most challenging and life-threatening diseases to treat.^{1,2} According to the World Health Organization, it is the second leading cause of death, responsible for 10 million deaths in 2020,^{3,4} with this number expected to rise to 16.4 million by 2040.⁵ In response to the global cancer crisis, extensive efforts have been devoted to the development of new chemotherapeutic agents. However, these therapeutics are limited by low selectivity, reduced efficacy, significant toxicity, the emergence of drug resistance, and/or severe side effects. As a result, the discovery of new anticancer drugs has been a critical research focus in recent years.⁶

Angiogenesis is the process of forming new capillaries from pre-existing blood vessels.^{7,8} Although angiogenesis is essential for normal physiological processes such as embryogenesis, inflammation, and wound healing, it also plays a critical role in cancer progression.⁹ Dysregulated angiogenesis supplies oxygen and nutrients to cancerous cells, promoting their growth and eventually triggering metastasis.¹⁰ Consequently, inhibiting angiogenesis has emerged as a promising strategy to prevent tumor growth and invasion.¹¹

Vascular endothelial growth factors (VEGFs) are key activators in the early stages of angiogenesis.^{12,13} VEGF stimulates endothelial cell activation, proliferation, and migration and enhances vascular permeability in tumors.¹⁴ This process is mainly mediated by vascular endothelial growth factor receptor 2 (VEGFR-2), a specific receptor considered a critical target in anti-angiogenic cancer therapies.¹⁵

As a result, the FDA has approved several kinase and VEGFR-2 inhibitors for the treatment of various cancers. VEGFR-2 inhibitors can be classified into three categories based on their binding modes (Fig. 1).¹⁶ Type I inhibitors, such as sunitinib and nintedanib, competitively bind to the ATP pocket of VEGFR-2 in its active “DFG-in” conformation.^{17,18} In contrast, type II inhibitors, including

^a Medicinal Chemistry Department, Faculty of Pharmacy, Assiut University, Assiut 71526, Egypt. E-mail: adelfawzy@aun.edu.eg^b Department of Pharmaceutical Sciences, College of Pharmacy, University of Tennessee Health Science Center, Tennessee 38163, USA. E-mail: mkhalifa@uthsc.edu^c School of Cellular & Molecular Medicine, University of Bristol, University Walk, Bristol, BS8 1TD, UK^d University Hospitals Bristol and Weston, NHS Foundation Trust, Bristol, BS1 3NU, UK† Electronic supplementary information (ESI) available: The spectral data, biological investigation, and molecular modeling studies are available in the ESI. See DOI: <https://doi.org/10.1039/d5md00332f>

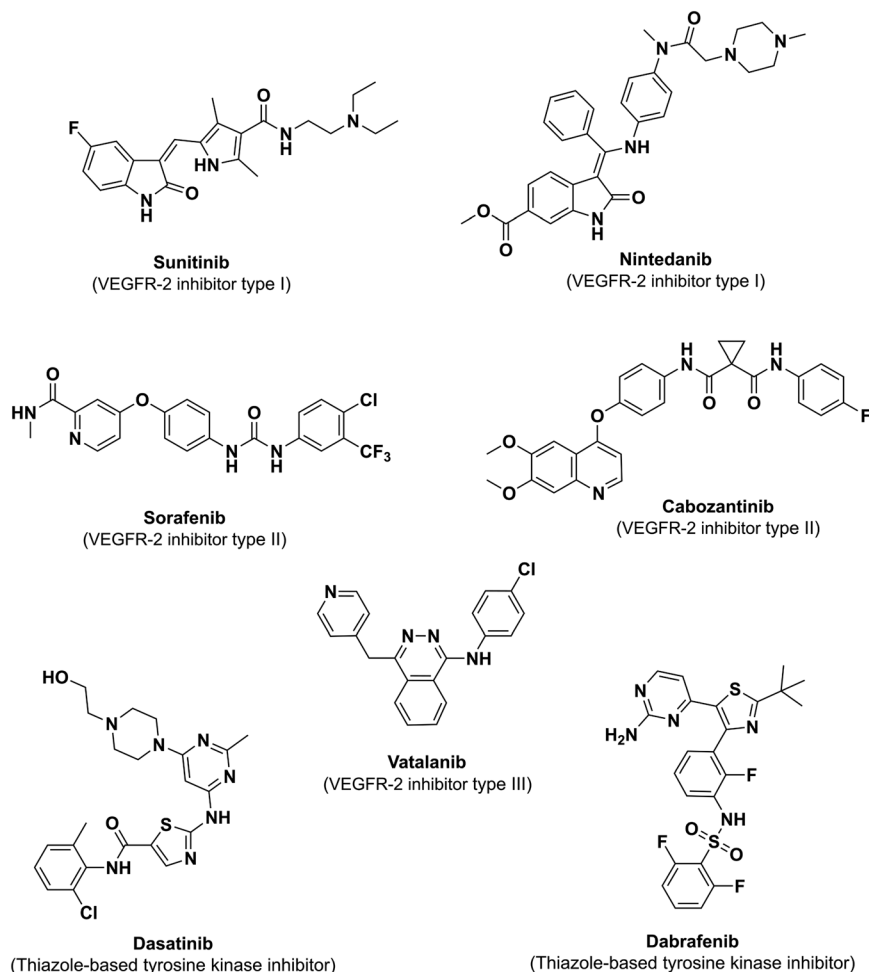


Fig. 1 Structures of different types of VEGFR-2 inhibitors and thiazole-based tyrosine kinase inhibitors.

sorafenib and cabozantinib, stabilize VEGFR-2 in its inactive “DFG-out” conformation.¹⁹ In this state, the DFG motif (aspartate–phenylalanine–glycine) flips out, enabling ligand binding at an allosteric site adjacent to the ATP binding pocket. Finally, type III inhibitors, such as vatalanib, are irreversible inhibitors that covalently bind to a cysteine residue at the ATP binding site, effectively blocking ATP binding.²⁰

The oxindole scaffold has attracted significant attention in anticancer research, with many derivatives being extensively studied for their VEGFR-2 inhibitory properties.²¹ Sunitinib, the first commercially available kinase inhibitor from the oxindole class, has been approved for treating gastrointestinal stromal tumors and renal cell carcinoma.²² Similarly, thiazoles are versatile chemical synthons with a wide range of biological activities, including anticancer, antimicrobial, and anti-inflammatory effects.^{23,24} Several thiazole-based compounds have been developed to target cancer-related pathways, such as the FDA-approved drugs dabrafenib and dasatinib, which are selective tyrosine kinase inhibitors with potent antitumor activities (Fig. 1).²⁵ This study focuses on integrating the two privileged scaffolds, oxindole and thiazole, to create

novel hybrids with enhanced antiproliferative and VEGFR-2 inhibitory activities.²²

Rationale and molecular design

Extensive studies on the pharmacophoric features of VEGFR-2 inhibitors have four key elements essential for their activity.²⁶ First, a flat heteroaromatic ring occupies the ATP-binding domain and forms hydrogen bonds with Cys919 and Glu917 in the hinge region. Second, a central aryl ring serves as a bridge, connecting the hinge region to the DFG domain.²⁷ Third, a hydrogen bond acceptor and donor (HBA-HBD) moiety interacts with the DFG domain of the receptor.^{28,29} Finally, a terminal hydrophobic group engages the allosteric hydrophobic pocket through various hydrophobic interactions, as illustrated in Fig. 2.³⁰

Building on these findings and our ongoing efforts to discover potent antitumor agents, we employed a ligand-based drug design approach to develop new VEGFR-2 inhibitors.^{31–33} In the sight of aforementioned the four essential pharmacophoric features of VEGFR-2 inhibitors and bioisosteric modifications through integration of indolin-2-one and thiazole moieties, a library of molecules was

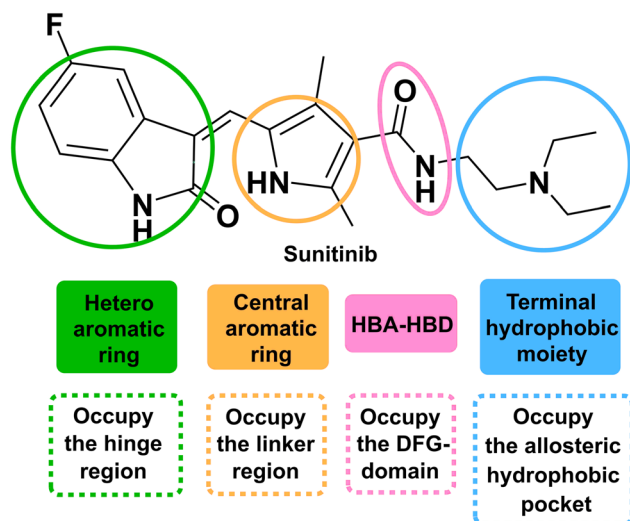


Fig. 2 Key pharmacophoric features of sunitinib as an example of a VEGFR-2 inhibitor.

designed and docked into the active site of VEGFR-2. Based on the results, a series of thirty-six indolin-2-one thiazole derivatives synthesized based on the synthetic feasibility and predicted as encouraging VEGFR-2 inhibitors. In this design, the indolin-2-one moiety was retained as the heteroaromatic feature to occupy the hinge region, where it effectively forms hydrogen bonds with Glu917 and Cys919 residues.³⁴ The thiazole ring served as the central aromatic linker between the indolin-2-one and the HBA-HBD functionality. To target the DFG domain, various groups such as amide,³⁵ hydrazide,³⁶ oxadiazole, and thiosemicarbazide,³⁷ were incorporated as HBA-HBD pharmacophoric features. These groups were chosen to accommodate different binding modes while modulating structural rigidity. Finally, a variety of aliphatic and aromatic hydrophobic groups were introduced to occupy the allosteric hydrophobic pocket,^{36–39} as shown in Fig. 3.

2. Results and discussion

2.1. Chemistry

The synthetic pathways for preparing the target compounds are outlined in Schemes 1–3. The structures of all newly synthesized compounds were confirmed through spectral and elemental analyses. Scheme 1 outlines the synthesis of key intermediates, ester **2** and hydrazide **3**. Initially, thiosemicarbazone **1** was synthesized by condensing isatin with thiosemicarbazide in refluxing absolute ethanol under acid catalysis, following a reported procedure.⁴⁰ The thiazole ring was introduced using the Hantzsch thiazole protocol by reacting **1** with ethyl bromopyruvate in refluxing absolute ethanol,^{41,42} yielding ester **2** in 90%. Finally, hydrazide **3** was obtained in 95% yield through hydrazinolysis of ester **2** with hydrazine hydrate.^{43–45}

The preparation of target derivatives **4a–o** and **5a–c** is depicted in Scheme 2. Schiff bases **4a–o** were synthesized in 70–90% yield by condensing hydrazide **3** with various aromatic aldehydes and ketones in absolute ethanol, using glacial acetic acid as a catalyst.^{46–48} Furthermore, cyclic imides **5a–c** were obtained in 80–86% yields through the cyclodehydration of hydrazide **3** with different acid anhydrides in toluene under reflux for 18–24 hours.^{49,50}

The synthesis of the target derivatives **6a–d**, **7a–d**, **8**, **10**, **11**, and **12a–e** is detailed in Scheme 3. Thiosemicarbazides **6a–d** were synthesized by reacting hydrazide **3** with different isothiocyanates in refluxing ethanol for 18–24 hours, resulting in the desired products in 68–81% yield.⁵¹ Cyclodesulfurization of **6a–d** was then achieved by treatment with potassium bisulfate in DMSO, producing oxadiazole derivatives **7a–d** in yields ranging from 62% to 67%. Additionally, heating hydrazide **3** at 100 °C with ammonium thiocyanate in dimethylformamide (DMF) with a few drops of hydrochloric acid yielded thiosemicarbazide **8** in 83%. This intermediate was subsequently cyclized with 4-bromophenacyl bromide **9a** in refluxing ethanol for 10

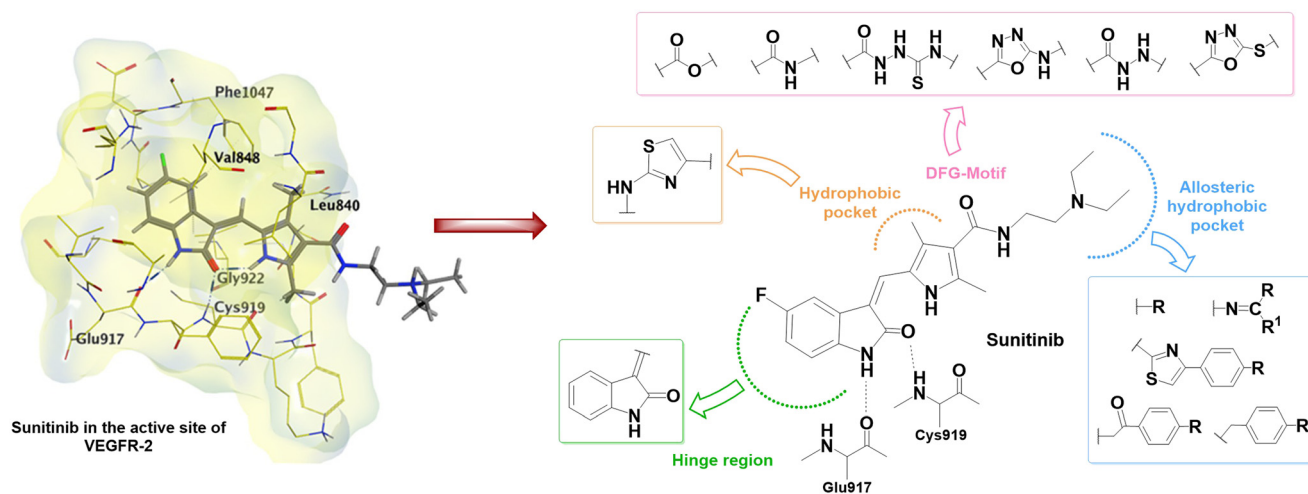
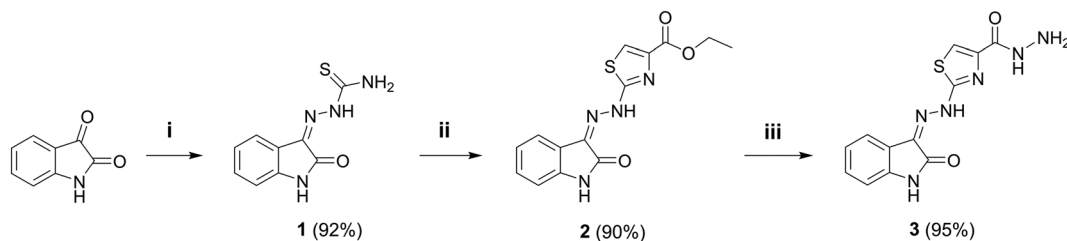
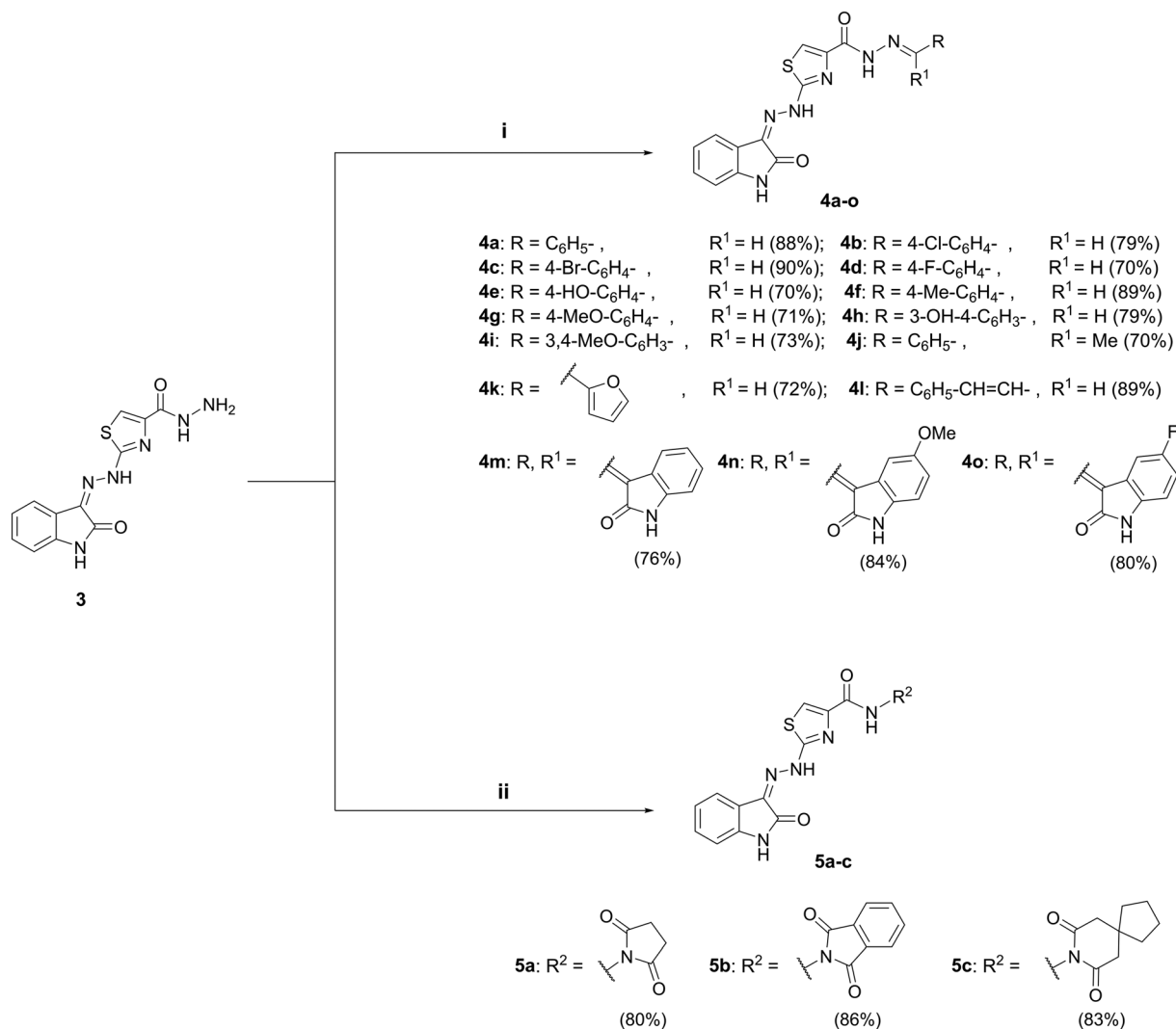


Fig. 3 Design of the target compounds based on the four key pharmacophoric features of VEGFR-2 inhibitors, using sunitinib as a lead compound.



Scheme 1 Synthesis of derivatives **1–3**. Reaction conditions: (i) thiosemicarbazide, EtOH, HCl, reflux, 3 h; (ii) ethyl bromopyruvate, EtOH, reflux, 12 h; (iii) hydrazine hydrate, EtOH, reflux, 24 h.



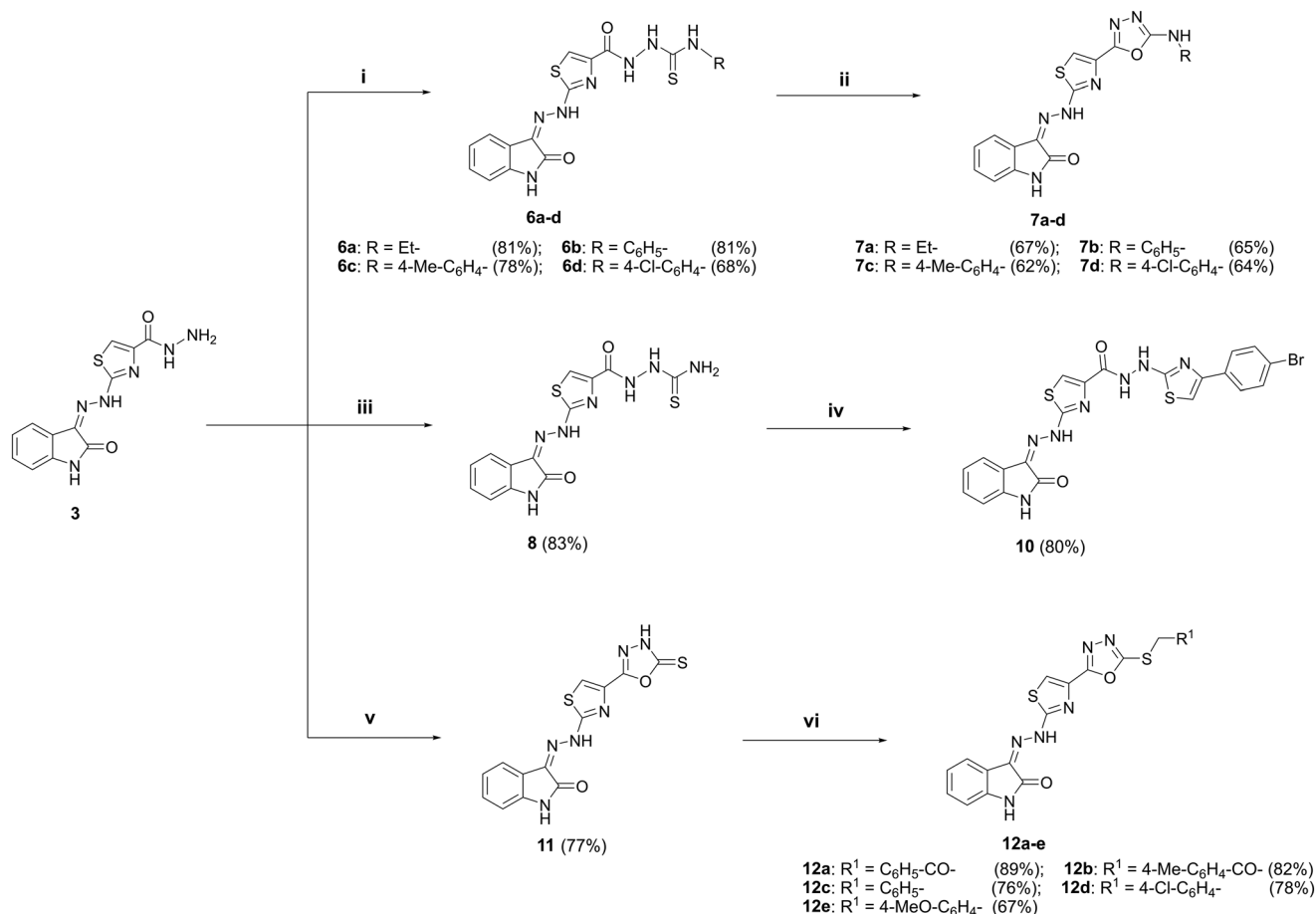
Scheme 2 Synthesis of **4a–o** and **5a–c**. Reaction conditions: (i) RCOR¹, EtOH, AcOH, reflux, 18–30 h; (ii) acid anhydride, PhCH₃, reflux, 18–24 h.

hours, yielding thiazole derivative **10** in 80%.⁵² Hydrazide **3** was subjected to cyclization conditions with carbon disulfide and potassium hydroxide followed by acidification to provide the 1,3,4-oxadiazole-2-thione **11** in 77% yield. Reacting compound **11** with phenacyl bromide **9b**, **c** produced **12a** and **12b** in 89% and 82% yield, respectively. Additionally, compound **11** was *S*-alkylated with several benzyl chlorides to afford target compounds **12c–e** in 67–78% yield.⁵³

2.2. Biological investigations

2.2.1. *In vitro* antiproliferative screening against NCI cancer cell lines

2.2.1.1. *In vitro* single-dose anticancer assay. Following the initial antiproliferative screening conducted at Bristol University against the MDA-MB-231 breast cancer cell line (see ESI,[†] Fig. S37–S39), the synthesized compounds



Scheme 3 Synthesis of **6a-d**, **7a-d**, **8**, **10**, **11**, and **12a-e**. Reaction conditions: (i) R-SCN, EtOH, reflux, 18–24 h; (ii) KHSO₄, DMSO, 50 °C, 36–48 h; (iii) NH₄SCN, DMF, HCl, 100 °C, 24 h; (iv) 4-Br-C₆H₄-COCH₂Br **9a**, EtOH, reflux, 10 h; (v) (a) CS₂, KOH, EtOH, reflux, 24 h, (b) 10% HCl; (vi) R¹-CH₂Br **9b**, c/R¹-CH₂Cl, MeCN, K₂CO₃, rt, 6–8 h.

demonstrated moderate to potent cytotoxic activity, compared to the reference drug sunitinib. Compounds **4c** and **4l** exhibited the most potent antiproliferative effects, while among the thiosemicarbazide derivatives, **6c** showed a strong cytotoxic response. Based on these promising results, the compounds were further submitted to the National Cancer Institute (NCI) for comprehensive *in vitro* anticancer evaluation.

The NCI selects compounds for *in vitro* anticancer screening based on specific criteria, which include drug-like properties, the novelty of the heterocyclic ring system, and integration with computer-aided drug design. Compounds containing undesirable moieties or linkages, such as nitroso, azo, and flexible acyclic groups are excluded from consideration. According to NCI protocols (NCI, USA, https://dtp.cancer.gov/discovery_development/nci-60/methodology.htm), the target compounds were tested at a single concentration of 10 μM against a panel of 60 human cancer cell lines from nine different human tissues.⁵⁴ The antiproliferative results for each compound were presented as cell growth percentage of the treated cancer cells in comparison to the untreated negative control cells^{55,56} (see ESI,† Tables S1–S4 and Fig. S40–S75).

The anticancer screening data for the synthesized compounds are reported as percentage growth inhibition against the treated cell lines (Tables 1–3). The growth inhibition percentage (GI%) was calculated by subtracting the cell growth percentage from 100. According to the NCI results, Compounds **4b**, **4c**, **4d**, and **4l** demonstrated complete cell death across the tested cell lines, with mean growth inhibition percentages of 118.86%, 135.32%, 148.27%, and 126.16%, respectively. Additionally, compound **6c** exhibited potent cytotoxicity, with mean growth inhibition percentage of 78.46% across multiple cancer cell lines. Moreover, compounds **4f** and **4g** exhibited moderate activity against some investigated cell lines, as showed in Table 1.

Compound **4b** induced total cell death across most tested cell lines, with growth inhibition percentages ranging from 100.74% to 186.25%. It showed strong antiproliferative activity against leukemia (SR) cell line, colon cancer (HCT-15, HT-29) cell lines, CNS cancer (SF-268, SNB-19) cell lines, melanoma (M14, MDA-MB-435) cell lines, renal cancer (SN12C) cell line, and breast cancer (BT-549) cell line, with growth inhibition values of 81.11%, 96.53%, 97.60%, 81.63%, 95.40%, 82.51%, 99.09%, 88.63%, and 98.53%, respectively.

Table 1 Cytotoxicity screening represented in growth inhibition percentage (GI%) for compounds **2**, **3**, and **4a–j** at a single-dose of 10 μ M against a panel of sixty cancer cell lines

Subpanel/cancer cell lines	Growth inhibition percentage (GI%)											
	2	3	4a	4b	4c	4d	4e	4f	4g	4h	4i	4j
Leukemia												
CCRF-CEM	5.12	18.75	4.92	56.19	67.81	94.63	19.98	11.67	59.73	8.11	26.29	5.35
HL-60(TB)	7.11	15.69	−0.47	30.32	70.17	95.57	8.02	16.08	50.50	1.72	16.16	10.60
K-562	3.92	2.88	−4.32	79.57	104.65	123.97	−2.16	13.06	33.68	14.49	16.98	−4.33
MOLT-4	6.77	2.95	−9.35	51.29	77.93	94.17	5.21	8.88	62.66	6.25	6.99	−4.72
RPMI-8226	15.03	−1.19	3.41	66.35	77.20	125.95	12.41	12.03	65.31	23.38	41.69	12.44
SR	NA	NA	7.99	81.11	134.89	115.87	15.17	29.80	47.89	6.60	42.28	13.73
Non-small cell lung cancer												
A549/ATCC	4.05	1.57	2.60	156.33	175.72	125.68	−5.46	53.89	70.70	19.52	16.99	4.76
EKVX	8.94	2.94	−0.39	115.58	156.36	178.86	−15.16	16.71	11.10	−2.77	−0.31	7.60
HOP-62	−5.01	0.76	−27.22	159.95	119.00	152.64	−17.11	86.38	89.82	−36.69	3.14	5.99
HOP-92	5.66	−0.42	−30.86	142.31	148.17	140.52	−53.99	23.86	14.99	−5.37	3.83	−15.06
NCI-H226	11.31	21.89	−16.63	115.13	128.91	88.92	−17.50	135.80	145.50	−0.42	52.98	22.36
NCI-H23	2.36	−1.77	−1.33	129.41	163.96	182.64	−0.10	29.59	31.46	17.90	15.45	4.78
NCI-H322M	−27.7	−1.54	−33.73	73.22	84.12	17.27	−29.35	−10.30	−0.60	−14.33	−8.42	−8.01
NCI-H460	2.03	−10.46	−4.12	160.25	169.66	164.90	−2.98	21.02	32.55	−0.20	20.12	−22.07
NCI-H522	4.44	6.48	15.40	75.45	154.49	167.37	11.94	42.69	56.36	24.19	10.30	10.00
Colon cancer												
COLO 205	6.86	6.88	2.13	154.24	103.32	94.68	4.58	4.13	12.11	−12.14	3.72	12.21
HCC-2998	−5.09	−2.87	−8.58	113.45	128.25	184.61	−9.64	8.90	12.86	−0.95	−2.71	−9.27
HCT-116	4.96	6.95	2.47	136.86	95.46	91.43	0.01	44.5	61.85	5.65	14.66	−3.59
HCT-15	8.83	0.22	0.35	96.53	149.10	185.03	−0.06	3.70	8.99	−3.14	2.56	5.75
HT29	6.65	1.61	9.38	97.60	187.34	181.31	3.15	22.05	51.26	2.31	−14.79	8.15
KM12	0.63	0.97	−1.33	100.74	132.84	109.59	−1.11	2.54	14.09	−4.02	0.79	−9.27
SW-620	−9.29	−17.77	−11.91	164.16	166.89	163.65	−11.50	4.85	22.14	−11.35	0.91	−18.79
CNS cancer												
SF-268	−0.78	4.66	−11.55	81.63	79.88	124.39	−15.90	28.14	41.94	−11.40	8.00	−1.62
SF-295	3.58	4.02	2.74	133.78	156.24	181.11	−4.14	41.24	32.33	2.27	19.46	2.23
SF-539	0.37	4.69	−5.69	130.88	182.47	169.05	−3.20	94.21	120.73	16.38	44.58	7.70
SNB-19	6.43	−0.78	−0.94	95.40	110.32	140.71	−7.20	84.05	81.68	4.28	30.22	2.47
SNB-75	NA	NA	−7.15	128.74	140.22	136.26	−5.68	131.74	129.14	−4.15	12.78	NA
U251	−0.24	2.79	−3.13	180.67	191.48	184.23	−7.50	46.85	58.78	11.79	29.31	−2.33
Melanoma												
LOX IMVI	1.95	16.44	−6.93	186.25	195.19	188.82	−6.14	37.50	27.46	3.13	−0.51	3.69
MALME-3M	−9.99	−12.93	−6.73	143.73	152.95	190.46	−6.57	9.09	35.43	−8.68	10.78	−8.74
M14	1.60	−1.21	−5.14	82.51	98.54	97.42	−8.10	15.04	16.58	−10.20	−1.41	6.94
MDA-MB-435	7.34	4.93	0.80	99.09	155.20	162.78	−0.41	14.29	41.49	−0.73	8.77	NA
SK-MEL-2	−0.63	−10.22	−1.86	126.26	114.20	165.86	−9.49	9.05	18.20	6.28	−6.21	−7.27
SK-MEL-28	−1.72	−5.90	−6.97	122.85	153.88	157.43	−12.28	22.07	30.72	0.63	−7.66	14.82
SK-MEL-5	4.97	5.58	2.67	78.46	169.35	180.41	5.75	45.44	69.13	21.88	25.39	9.78
UACC-257	0.60	3.41	−2.84	58.91	70.47	132.24	−4.64	2.62	11.31	3.36	−5.89	1.80
UACC-62	4.45	1.44	1.42	NA	135.11	138.97	−6.50	38.68	32.26	NA	0.67	3.30
Ovarian cancer												
IGROV1	−16.33	−22.72	−27.59	109.45	166.76	181.49	−28.61	−18.11	−22.16	−6.83	−19.05	−12.62
OVCAR-3	−1.48	−7.91	−16.67	184.90	183.27	194.19	−15.00	−4.35	33.63	−18.25	−15.35	−19.36
OVCAR-4	NA	NA	9.23	135.70	122.49	158.48	12.48	65.44	77.38	−3.62	19.84	NA
OVCAR-5	−3.76	−3.38	−6.89	110.83	110.58	169.70	−32.36	17.62	6.77	−32.28	2.10	−6.31
OVCAR-8	−2.74	−3.87	−0.88	142.01	122.09	181.35	14.07	69.27	87.49	30.34	31.49	2.67
NCI/ADR-RES	4.07	−6.00	−6.51	146.23	161.54	168.75	−8.41	73.45	84.13	10.03	15.24	1.32
SK-OV-3	−23.18	−11.87	−9.42	166.17	102.08	149.29	−1.19	11.07	23.95	−12.72	−10.06	21.01
Renal cancer												
786-0	14.45	7.93	18.87	143.67	145.15	168.89	12.77	51.47	64.78	7.46	3.16	3.85
A498	−4.20	−4.39	−10.25	138.79	171.72	190.10	−31.00	−49.45	−34.86	8.34	−15.67	−21.62
ACHN	−4.10	5.58	−5.47	121.92	150.21	174.23	−8.19	43.08	58.11	3.19	6.77	14.29
CAKI-1	13.19	5.81	9.02	157.59	177.57	168.57	0.05	60.25	64.26	13.16	11.86	NA
RXF 393	−3.83	−0.94	−11.56	114.36	177.82	191.42	−20.95	107.64	108.26	8.44	25.12	5.24
SN12C	−2.76	−1.25	−2.13	88.63	123.17	137.82	−3.66	68.02	66.71	12.93	10.03	7.10
TK-10	−12.47	−17.32	10.95	138.96	140.03	176.10	−31.32	2.03	0.27	−6.25	−39.17	−19.38
UO-31	8.82	7.65	3.25	145.44	173.26	191.04	8.64	46.12	61.61	−1.43	20.24	10.31
Prostate cancer												
PC-3	6.84	2.67	−3.55	105.23	140.79	131.57	−1.15	22.78	28.30	6.72	9.95	−0.82
DU-145	−3.26	−2.74	−5.34	156.35	126.56	144.25	−8.18	28.36	39.37	−1.76	11.63	−2.19

Table 1 (continued)

Subpanel/cancer cell lines	Growth inhibition percentage (GI%)											
	2	3	4a	4b	4c	4d	4e	4f	4g	4h	4i	4j
Breast cancer												
MCF7	8.03	10.89	4.79	106.15	120.89	159.87	2.90	12.11	28.46	0.90	7.78	16.77
MDA-MB-231/ATCC	−8.05	23.65	−0.35	152.30	164.72	150.67	−3.49	67.27	63.63	5.76	28.86	6.18
HS 578T	−9.44	−17.64	−17.00	104.62	99.01	66.52	−21.29	41.08	70.72	−17.50	20.78	−10.88
BT-549	−4.24	5.12	11.77	98.53	116.33	116.05	−12.66	23.15	63.55	−3.90	3.61	5.60
T-47D	9.50	7.76	10.29	128.48	92.51	114.53	15.59	26.36	59.51	23.07	11.67	25.91
MDA-MB-468	−1.06	−11.93	−16.93	111.08	129.05	182.18	−2.73	26.86	29.17	−36.80	−0.79	11.42
MEAN% GI	0.69	0.64	−3.59	118.86	135.32	148.27	−5.69	33.22	46.09	1.06	9.63	1.78

NA; not available.

Compound **4c** induced lethality in most tested cell lines, with growth inhibition percentages between 100.99% and 195.19%. It showed maximum growth inhibition against melanoma (LOX IMVI) cell line and minimum against leukemia (CCRF-CEM) cell line, with GI% values of 195.19% and 67.81%, respectively. Additionally, **4c** demonstrated potent growth inhibition against non-small cell lung cancer (NCI-H322M) cell line, colon cancer (HCT-116) cell line, melanoma (M14) cell line, and breast cancer (HS 578T, T-47D) cell lines, with GI% values of 84.12%, 95.46%, 98.54%, 99.01%, and 92.51%, respectively.

The target derivative **4d** induced complete cell death across most tested cell lines, with growth inhibition percentages ranging from 109.59% to 194.19%. It displayed broad-spectrum antitumor activity against leukemia cell lines, with GI% values from 94.17% to 125.95%. Moreover, **4d** exhibited significant anticancer activity against non-small cell lung cancer (NCI-H226) cell line, colon cancer (COLO 205, HCT-116) cell lines, and melanoma (M14) cell line, with GI% values of 88.92%, 94.68%, 91.43%, and 97.42%, respectively.

Compound **4l** demonstrated significant cytotoxicity across all tested cell lines, with growth inhibition percentages between 100.55% and 191.59%. It showed a broad growth inhibitory effect against ovarian cancer (OVCAR-8) cell line, with a GI% value of 186.01% and exhibited strong growth inhibition above 90% against non-small cell lung cancer (NCI-H522) cell line, ovarian cancer (IGROV1) cell line, and breast cancer (HS 578T) cell line.

Compound **6c** induced cell death in several tested cell lines, with growth inhibition percentages ranging from 108.56% to 192.86%. It showed exceptional antiproliferative activity against CNS cancer (SF-295) cell line, with growth inhibition percentage of 192.86%. In addition, **6c** displayed potent growth inhibition across leukemia, non-small cell lung cancer, colon cancer, CNS cancer, melanoma, ovarian cancer, renal cancer, prostate cancer, and breast cancer cell lines, with GI% values up to 99.47%.

Structure–activity relationship (SAR) analysis of the synthesized compounds demonstrated that the molecular hybridization of isatin as the heteroaromatic feature and thiazole as the central aromatic linker produced efficient

antitumor derivatives (Fig. 4). Among the different HBA-HBD functionalities, the hydrazide spacer exhibited the most potent antiproliferative activity, followed by thiosemicarbazide. In contrast, cyclization of the HBA-HBD group into an oxadiazole ring, as observed in derivatives **7a–d**, and **12a–e** led to reduced cytotoxicity. This decrease in activity is likely due to the steric rigidity and limited rotational freedom of the oxadiazole ring within the DFG domain of the VEGFR-2 active site.

The absence of a hydrophobic moiety, as seen in compounds **3**, **8**, and **11**, led to a significant decrease in cytotoxic activity, emphasizing the critical role of this feature in facilitating effective interaction with the allosteric hydrophobic pocket of VEGFR-2. In the series of Schiff bases **4a–o**, halogen-substituted hydrazones **4b–d** displayed more potent and broader antiproliferative activity compared to their non-halogenated counterparts. Furthermore, the introduction of extended conjugation in the hydrophobic feature, as demonstrated by compound **4l**, notably enhanced cytotoxic activity. On the other hand, the incorporation of polar substituents, as in compounds **4e** and **4h**, resulted in less pronounced activity. Among the carboxamide derivatives, compounds **5a** and **5c**, containing aliphatic moieties, exhibited greater cytotoxic effects than compound **5b**, which featured an aromatic moiety.

2.2.1.2. In vitro five-dose anticancer assay. Based on the preliminary screening results, compounds **4b**, **4c**, **4d**, **4l**, and **6c** were selected by the NCI for further evaluation at five-dose concentrations (0.01, 0.1, 1, 10, and 100 μ M) due to their strong cytotoxic activity against various cancer cell lines. The results were used to generate log concentration vs. percentage growth curves, from which three dose response parameters (GI_{50} , TGI, and LC_{50}) were calculated for each cell line (see ESI,[†] Table S5 and Fig. S76–S81). Growth inhibition concentration of 50% (GI_{50}) represents the concentration at which 50% growth inhibition occurs. Total growth inhibition (TGI) is the drug concentration resulting in total growth inhibition and indicates complete cytostatic activity. The lethal concentration of 50% (LC_{50}) is the concentration of drug resulting in a 50% net cell loss and reflects the cytotoxicity of the compounds. The investigated Schiff base derivatives **4b**, **4c**, **4d**, **4l**, and the thiosemicarbazide

Table 2 Cytotoxicity screening represented in growth inhibition percentage (GI%) for compounds **4k-o**, **5a-c**, and **6a-d** at a single-dose of 10 μ M against a panel of sixty cancer cell lines

Subpanel/cancer cell lines	Growth inhibition percentage (GI%)											
	4k	4l	4m	4n	4o	5a	5b	5c	6a	6b	6c	6d
Leukemia												
CCRF-CEM	20.60	68.42	2.49	8.62	23.40	4.26	-2.42	3.69	52.37	-19.44	65.88	10.29
HL-60(TB)	1.39	78.81	-2.83	5.19	-8.30	17.95	-1.74	16.12	23.92	10.60	27.88	8.86
K-562	-0.90	106.79	-10.40	7.30	4.41	-2.69	-9.64	27.27	45.67	5.27	64.61	3.28
MOLT-4	4.49	118.66	-5.23	19.14	2.13	-6.28	-14.44	25.31	27.09	9.57	44.71	3.00
RPMI-8226	30.02	86.52	4.02	-16.93	7.73	6.60	0.55	15.10	21.18	-3.99	32.57	7.05
SR	NA	101.60	2.91	8.25	18.84	22.42	-4.20	24.53	NA	10.93	72.38	11.43
Non-small cell lung cancer												
A549/ATCC	3.76	160.38	0.11	11.33	-2.53	0.52	-2.29	12.48	-0.77	-1.61	58.42	7.20
EKVX	-1.12	120.40	0.79	14.57	-0.94	-5.08	1.66	23.66	9.36	-6.41	99.76	10.01
HOP-62	-5.65	120.64	5.00	18.55	-12.38	-0.64	6.60	-28.83	36.17	-4.59	64.31	0.42
HOP-92	-21.60	115.30	-9.48	41.23	-4.19	-9.00	-15.65	6.75	14.54	6.69	99.47	2.64
NCI-H226	0.11	83.00	9.02	-20.06	5.29	13.77	4.93	-5.37	29.6	-3.89	114.31	11.75
NCI-H23	2.76	144.59	7.20	19.28	5.62	0.84	3.36	3.10	13.36	6.02	91.18	0.65
NCI-H322M	-28.78	66.25	-6.79	-64.32	-17.00	-11.27	-18.63	-47.27	25.01	-15.44	51.63	-6.09
NCI-H460	-12.62	161.24	-18.59	-18.49	-20.26	-26.11	-4.04	-14.34	10.76	-8.60	77.69	-8.32
NCI-H522	3.06	93.67	7.88	9.66	19.20	5.44	5.44	14.29	5.97	11.78	94.95	15.34
Colon cancer												
COLO 205	-7.72	79.34	6.62	-17.05	19.28	8.03	-5.35	-12.12	-2.62	-14.01	17.52	6.30
HCC-2998	0.67	116.30	-2.31	-9.47	-5.98	-6.57	-11.17	-1.47	17.29	-1.03	129.06	-0.55
HCT-116	3.91	176.16	-6.05	2.79	-2.59	5.93	2.78	-1.59	27.19	-6.11	63.56	-6.05
HCT-15	2.80	107.49	2.32	-4.91	7.39	-2.69	0.50	2.34	56.04	-10.23	127.03	6.07
HT29	11.49	146.40	-0.94	-2.49	1.57	-9.80	1.03	-2.92	2.22	5.03	36.72	5.36
KM12	-2.47	89.92	-10.25	-3.94	-21.93	-3.16	-1.56	-1.89	7.09	-3.33	89.05	-2.73
SW-620	-15.70	163.11	-29.15	4.86	2.62	-24.86	-6.03	-22.22	-3.76	-9.42	52.62	3.71
CNS cancer												
SF-268	-2.09	79.19	0.65	25.76	-7.49	-1.30	-4.73	-1.52	26.04	-6.88	70.19	8.20
SF-295	0.75	125.45	-2.09	61.42	-0.56	1.96	1.01	-0.16	20.63	-5.04	192.86	7.47
SF-539	3.03	170.00	2.09	13.52	4.75	2.52	-2.95	4.15	16.53	-0.85	165.62	0.75
SNB-19	10.65	109.49	1.40	42.85	4.63	0.28	-0.11	7.11	19.62	2.18	82.69	20.55
SNB-75	NA	137.76	-10.21	-39.90	13.66	6.31	20.32	5.70	NA	-0.64	112.72	9.59
U251	-0.99	190.80	-0.34	39.58	-1.78	-0.59	2.27	5.49	35.8	-2.50	66.91	6.69
Melanoma												
LOX IMVI	-1.51	181.34	9.02	3.16	12.34	-1.17	3.99	-2.08	26.65	-2.58	148.79	6.20
MALME-3M	-26.66	188.11	-6.74	7.90	-5.81	-24.24	-7.55	10.08	13.44	-22.28	85.96	-0.16
M14	8.54	88.80	5.05	-0.45	1.99	9.93	-2.48	0.86	27.62	-10.38	67.77	3.38
MDA-MB-435	5.55	142.37	-6.56	18.11	1.66	-1.16	-0.97	4.95	22.38	0.83	75.38	3.45
SK-MEL-2	4.44	77.21	-5.30	0.34	1.43	-10.86	-11.14	-6.25	17.39	1.70	79.44	-4.35
SK-MEL-28	-1.46	133.98	-0.84	-4.57	1.59	-4.86	-7.88	-1.16	21.12	-4.04	60.44	-0.30
SK-MEL-5	3.79	88.04	10.31	13.6	-1.14	5.96	-0.71	28.40	74.89	7.25	186.82	2.47
UACC-257	6.80	100.55	3.76	10.35	-1.08	0.63	-3.98	20.00	4.46	0.19	28.67	7.04
UACC-62	5.56	NA	3.72	NA	6.68	5.31	1.69	NA	26.11	NA	128.67	7.89
Ovarian cancer												
IGROV1	-34.31	99.91	-12.27	15.00	-14.19	-23.28	-23.70	1.35	4.73	-36.76	56.66	-8.17
OVCAR-3	-5.48	191.59	-22.71	54.64	-2.88	-8.38	-6.88	-4.02	28.49	-18.63	60.70	-9.08
OVCAR-4	NA	173.16	-8.43	52.02	4.23	-7.36	3.09	9.67	NA	-4.65	72.48	0.57
OVCAR-5	0.34	143.10	-4.34	-11.93	-3.99	-7.43	-7.73	-6.65	20.42	-3.51	32.79	-5.08
OVCAR-8	1.89	186.01	8.46	4.16	-1.11	-1.19	-2.76	2.10	18.74	1.37	74.22	8.37
NCI/ADR-RES	-1.75	163.20	0.88	2.28	6.95	2.46	-4.49	7.70	11.51	-0.01	44.83	7.63
SK-OV-3	-12.16	113.19	11.46	0.58	-7.59	4.78	-15.43	-13.41	4.84	-7.49	24.70	14.07
Renal cancer												
786-0	9.30	168.08	6.57	33.07	-10.61	10.88	8.27	15.82	29.3	6.35	40.85	10.39
A498	0.52	58.66	-34.42	-32.79	-23.56	-51.03	-15.72	-3.00	17.88	-0.31	8.26	-5.68
ACHN	-6.20	136.43	6.46	9.48	4.71	-9.77	-2.74	-7.01	48.92	-3.68	67.83	5.75
CAKI-1	4.70	115.74	15.48	-6.64	9.85	4.47	11.37	-0.43	53.11	3.53	126.29	13.65
RXF 393	-2.02	100.71	2.96	-35.61	-3.75	2.10	-4.56	-32.48	18.18	-29.59	108.56	13.25
SN12C	9.61	131.46	-5.20	10.35	1.29	-0.37	-1.68	13.27	10.92	6.81	62.58	10.11
TK-10	-6.51	158.21	-15.57	-23.87	-25.43	-13.15	-28.72	3.03	53.72	-23.20	61.03	-6.22
UO-31	5.51	153.36	11.82	-25.27	20.13	7.65	-4.96	-7.49	55.45	15.39	60.34	14.61
Prostate cancer												
PC-3	4.84	112.47	3.51	-0.16	5.47	3.05	5.65	8.01	33.08	-11.48	65.58	2.14
DU-145	4.25	125.32	-17.87	28.20	-3.58	-13.06	-8.38	-9.89	14.43	-10.83	59.26	-2.56

Table 2 (continued)

Subpanel/cancer cell lines	Growth inhibition percentage (GI%)											
	4k	4l	4m	4n	4o	5a	5b	5c	6a	6b	6c	6d
Breast cancer												
MCF7	5.75	150.58	9.19	13.85	4.18	1.66	6.93	1.13	14.16	−8.04	90.26	1.50
MDA-MB-231/ATCC	1.77	156.89	10.56	21.14	5.37	0.96	1.04	0.84	18.51	−6.25	97.59	9.96
HS 578T	−16.78	95.34	−0.83	18.95	−0.06	−24.56	−7.02	−4.89	0.97	−5.61	90.89	−11.20
BT-549	6.93	84.17	6.32	7.89	−9.64	3.97	−9.97	15.17	20.07	−0.20	69.45	14.20
T-47D	16.69	167.20	14.12	46.18	14.12	12.58	3.33	18.40	−4.91	4.19	54.23	18.77
MDA-MB-468	−12.61	140.47	4.79	3.58	5.55	1.51	−0.59	−4.71	15.38	−18.96	150.07	14.54
MEAN% GI	−0.37	126.16	−0.98	6.61	0.46	−2.29	−3.15	1.94	22.07	−4.01	78.46	4.67

NA; not available.

derivative **6c** had potent antiproliferative activities in the micromolar range across most of the tested cell lines representing the nine different subpanels (Table 4).

Generally, compound **4b** exhibited potent cytotoxic activity across most cancer cell lines. The highest activity was observed against non-small cell lung cancer (A549/ATCC, NCI-H460) cell lines, colon cancer (SW-620) cell line, CNS cancer (SF-295, SNB-75, U251) cell lines, melanoma (LOX IMVI) cell line, ovarian cancer (OVCAR-3, NCI/ADR-RES) cell lines, renal cancer (786-0, RXF 393) cell lines, prostate cancer (DU-145) cell line, and breast cancer (MDA-MB-231/ATCC, MDA-MB-468) cell lines, with GI_{50} of 2.13, 2.00, 2.06, 2.15, 1.88, 2.03, 2.04, 2.09, 2.09, 1.69, 2.02, 2.23, 2.22, and 1.86 μ M, respectively.

Compound **4c** revealed superior antiproliferative activity against most of the tested cell lines, with GI_{50} range from 1.71 to 5.88 μ M. Moreover, **4c** exhibited strong inhibition activity with GI_{50} values less than 2.00 μ M against non-small cell lung cancer (A549/ATCC, NCI-H23) cell lines, CNS cancer (SF-295, U251) cell lines, melanoma (LOX IMVI, SK-MEL-28) cell lines, ovarian cancer (NCI/ADR-RES) cell line, renal cancer (786-0, RXF 393), and breast cancer (MDA-MB-231/ATCC) cell line. On the other hand, **4c** showed the least activity amongst all selected compounds against leukemia (HL-60[TB]) cell line with GI_{50} 43.10 μ M.

Compound **4d** displayed comparable cytotoxicity against leukemia (RPMI-8226) cell line, ovarian cancer (NCI/ADR-RES) cell line, renal cancer (RXF 393) cell line, and breast cancer (MCF7) cell line, with GI_{50} values of 6.91, 5.02, 3.27, and 8.97 μ M, respectively. Compound **4l** revealed good inhibition activity against leukemia (SR) cell line, colon cancer (HT 29) cell line, CNS cancer (U251) cell line, melanoma (LOX IMVI) cell line, ovarian cancer (NCI/ADR-RES) cell line, renal cancer (786-0, RXF 393) cell lines, and breast cancer (MCF7, MDA-MB-231/ATCC) cell lines, with GI_{50} values of 2.46, 2.36, 2.92, 2.79, 2.77, 2.82, 2.79, 2.54, and 2.92 μ M, respectively.

Among the target compounds, **6c** displayed potent antiproliferative activity against leukemia (CCRF-CEM, K-562, and SR) cell lines, with GI_{50} values of 2.93, 3.39, and 2.70 μ M, respectively. Furthermore, **6c** showed potent cytotoxic activity across non-small cell lung cancer (HOP-92) cell line,

CNS cancer (SNB-75) cell line, renal cancer (RXF 393) cell line, and breast cancer (HS 578T) cell line, with GI_{50} values of 2.26, 1.67, 2.17, and 2.94 μ M, respectively.

Regarding the sensitivity of the selected compounds toward different cell lines, compounds **4c** and **4b** had a comparatively potent antiproliferative effect throughout the whole NCI panel, with effective growth inhibition full panel GI_{50} (MG-MID) values of 2.82 μ M and 2.95 μ M, respectively.

2.2.2. In vitro cytotoxicity screening against hepatocellular carcinoma (HepG2) and normal liver cell line (THLE-2). The growth inhibitory activities of the most potent compounds **4b**, **4c**, **4d**, **4l**, and **6c** were evaluated *in vitro* against hepatocellular carcinoma (HepG2) and transformed human liver epithelial-2 (THLE-2) using MTT assay with sunitinib as a reference drug. The HepG2 cell line has been selected for assessment of IC_{50} of the tested compounds since it highly expresses VEGFR-2 (ref. 57 and 58) and is not involved in the NCI 60 cancer cell line protocol. The results (Table 5) revealed that compounds **6c**, **4c**, **4d**, and **4b** have more potent cytotoxic activity ($IC_{50} = 3.13 \pm 0.1$, 5.67 ± 0.19 , 11.62 ± 0.38 , and 21.98 ± 0.72 μ M, respectively) compared to sunitinib ($IC_{50} = 23.44 \pm 0.77$ μ M). Furthermore, the target compounds displayed lower cytotoxicity against the normal THLE-2 cells than sunitinib (Table 5). The selectivity index (SI) values of compounds **4b**, **4c**, **4d**, **4l**, and **6c** were calculated to evaluate selectivity for HepG2 tumor cells over THLE-2 normal cells. Compared to sunitinib (SI = 1.15), compounds **4b**, **4c**, **4d**, **4l**, and **6c** displayed significantly higher SI values (1.80, 7.88, 3.49, 3.57, and 10.26, respectively), indicating more favourable safety profiles.

2.2.3. In vitro VEGFR-2 kinase inhibitory assay. The most potent antiproliferative compounds **4b**, **4c**, **4d**, **4l**, and **6c** were evaluated for VEGFR-2 kinase inhibition using sunitinib as a reference drug. The IC_{50} values, summarized in Table 6, revealed significant VEGFR-2 inhibition, ranging from 0.047 to 1.549 μ M. Notably, compound **4c** demonstrated the strongest VEGFR-2 inhibition, being 3.55 times more potent than sunitinib ($IC_{50} = 0.047 \pm 0.002$ μ M vs. 0.167 ± 0.007 μ M). Compounds **6c** and **4b** also exhibited superior inhibitory activities compared to sunitinib, with IC_{50} values of 0.089 ± 0.004 μ M and 0.113 ± 0.005 μ M, respectively. These results, in conjunction with the cytotoxicity data, suggest that

Table 3 Cytotoxicity screening represented in growth inhibition percentage (GI%) for compounds **7a–d**, **8**, **10**, **11**, and **12a–e** at a single-dose of 10 μ M against a panel of sixty cancer cell lines

Subpanel/cancer cell lines	Growth inhibition percentage (GI%)											
	7a	7b	7c	7d	8	10	11	12a	12b	12c	12d	12e
Leukemia												
CCRF-CEM	58.69	40.38	46.34	4.32	15.73	19.05	1.42	37.30	4.03	6.67	5.74	9.68
HL-60(TB)	45.57	25.62	1.70	−8.37	42.24	9.86	−18.88	−15.39	10.06	23.34	3.63	10.70
K-562	42.69	60.62	52.29	−7.86	0.31	3.37	−6.62	58.82	1.68	14.32	−0.03	1.27
MOLT-4	88.49	38.88	30.23	−4.90	11.85	14.75	−3.77	77.67	8.13	−2.57	−3.58	18.65
RPMI-8226	57.81	23.90	29.42	3.89	1.39	33.71	−8.30	12.86	2.76	3.68	−4.49	9.03
SR	NA	37.93	18.87	5.63	NA	NA	NA	62.34	11.68	20.29	31.50	1.90
Non-small cell lung cancer												
A549/ATCC	54.46	12.96	1.84	−9.68	5.85	−5.47	−4.40	8.69	1.15	9.70	7.31	13.09
EKVX	38.70	20.12	0.26	10.23	−0.72	2.21	4.83	20.08	4.67	5.28	1.39	10.21
HOP-62	31.09	−5.30	−0.21	4.29	−21.46	−7.50	12.35	−1.88	26.14	−5.74	36.98	22.20
HOP-92	38.31	32.90	−11.67	−34.26	−2.67	8.33	6.12	7.53	3.01	16.10	−3.77	0.04
NCI-H226	49.09	−5.51	0.80	7.29	10.60	8.78	6.04	−4.90	20.80	−10.08	6.74	24.38
NCI-H23	20.52	17.66	10.82	4.17	0.96	8.64	2.90	41.73	18.38	4.17	12.69	16.59
NCI-H322M	11.27	6.92	−5.30	0.14	−7.39	−27.69	−22.24	−53.37	−18.98	−31.93	−7.90	−18.31
NCI-H460	63.52	1.29	45.05	−30.92	−15.12	−22.95	−15.80	−10.17	−3.36	1.94	−14.13	3.66
NCI-H522	7.58	61.56	43.26	4.61	3.18	2.86	1.89	13.87	19.06	16.85	13.36	16.38
Colon cancer												
COLO 205	34.12	−9.38	−0.59	7.71	−6.41	−3.87	−4.58	−16.79	−5.64	−4.70	−1.37	−4.24
HCC-2998	13.78	13.12	2.50	−0.82	−9.40	−2.38	−15.54	−10.31	−3.57	4.05	−20.82	−4.41
HCT-116	20.81	22.04	45.36	5.35	−3.27	5.15	7.32	24.65	−8.12	0.57	16.06	3.20
HCT-15	38.20	5.78	1.20	1.46	0.36	−4.53	−4.96	35.53	0.30	0.34	6.32	1.03
HT29	16.94	0.33	−22.77	−11.38	−3.77	1.57	−6.28	13.72	−1.86	15.04	−9.92	0.05
KM12	12.54	1.62	8.39	2.93	1.01	3.27	−1.66	−3.11	−0.21	−2.50	−6.19	−0.49
SW-620	14.07	−7.13	−0.18	−29.15	−23.91	−23.45	−8.06	−13.65	−3.15	4.73	−19.18	3.49
CNS cancer												
SF-268	21.22	18.78	4.93	−1.84	−1.44	−4.97	−3.13	−7.59	−8.56	1.69	9.96	−3.88
SF-295	44.54	−4.43	9.60	3.05	−7.10	−13.29	−9.29	40.48	28.92	7.50	16.15	28.13
SF-539	35.42	17.02	1.70	−0.79	1.04	−1.36	7.38	154.50	34.85	44.91	34.49	32.08
SNB-19	30.89	49.25	60.48	5.68	0.72	18.41	−0.38	10.58	51.71	9.41	27.12	54.41
SNB-75	NA	13.21	22.06	10.83	NA	NA	NA	−27.20	13.42	3.36	13.60	−0.28
U251	37.85	72.56	69.38	−6.14	1.74	9.40	−1.17	9.60	26.25	4.76	24.13	40.40
Melanoma												
LOX IMVI	43.78	24.45	30.25	4.51	0.28	−0.05	8.93	53.67	14.59	10.24	5.29	19.73
MALME-3M	−18.08	−34.72	−9.16	−0.10	−11.91	−40.28	−24.19	−2.86	17.55	−4.13	−2.73	26.81
M14	15.32	−4.20	3.82	5.91	5.28	9.64	0.16	8.42	3.22	−2.00	10.80	11.22
MDA-MB-435	17.73	0.64	7.94	−3.22	−4.22	3.13	−5.13	2.50	−1.56	9.52	0.53	0.11
SK-MEL-2	8.15	35.86	4.33	−7.48	−8.32	0.24	0.81	−8.68	9.18	−7.12	5.88	5.83
SK-MEL-28	13.41	6.55	−8.85	−6.02	−7.35	−11.38	−18.01	−5.05	−11.94	13.65	−4.95	−3.90
SK-MEL-5	28.27	22.46	30.09	4.69	3.30	11.22	3.18	4.79	14.75	4.66	14.31	23.56
UACC-257	15.10	−4.90	−22.31	3.28	1.36	−3.04	0.84	9.52	−5.73	6.36	9.32	−4.07
UACC-62	36.87	NA	34.91	4.76	−2.59	−3.68	7.47	NA	12.17	NA	3.16	20.71
Ovarian cancer												
IGROV1	−21.24	−26.46	−8.84	−3.38	−12.28	−47.35	−34.59	9.34	−11.92	3.72	−32.91	−17.37
OVCAR-3	16.78	7.31	6.87	−16.47	−8.96	−9.61	−11.06	−4.03	−24.54	−10.44	−13.31	−12.69
OVCAR-4	NA	−4.73	22.76	−2.74	NA	NA	NA	−9.29	3.99	12.28	1.94	11.10
OVCAR-5	8.37	−4.30	−9.76	−0.42	−4.43	−24.73	−3.95	−10.96	−11.53	1.77	−11.89	−9.32
OVCAR-8	42.06	12.32	8.41	1.18	−2.43	8.71	−2.75	2.29	29.93	−0.85	17.94	1.90
NCI/ADR-RES	13.52	1.78	−4.99	2.26	−6.76	−13.22	−9.63	17.32	13.45	9.19	1.08	22.22
SK-OV-3	1.31	−6.97	−21.56	16.84	−1.74	−6.86	11.49	−10.75	−21.74	−16.68	4.19	−8.22
Renal cancer												
786-0	32.81	−4.37	8.55	−2.20	6.87	8.59	0.38	−6.92	29.59	6.39	42.55	39.70
A498	13.36	−19.07	−34.26	−15.14	−8.32	−12.71	−40.05	−34.11	−25.90	−7.29	−23.81	−30.97
ACHN	43.44	3.95	3.96	14.71	−3.50	−9.74	−1.66	−0.65	8.13	0.04	19.72	25.83
CAKI-1	40.45	−7.03	13.96	14.12	7.59	−3.59	7.18	5.85	16.66	−2.43	16.03	13.55
RXF 393	15.10	−52.98	2.26	0.03	−4.74	−5.65	−12.87	−22.18	18.33	−41.38	23.19	6.85
SN12C	40.79	7.55	2.33	1.41	−10.74	−3.49	−3.56	10.76	6.25	7.93	3.09	10.07
TK-10	31.87	−46.62	−31.96	−34.42	−24.69	−66.23	−54.09	−64.02	−41.80	−7.50	−2.64	−40.90
UO-31	30.78	9.63	9.37	19.81	5.38	−4.41	14.11	8.72	8.94	4.88	20.01	17.14
Prostate cancer												
PC-3	19.84	16.68	17.85	2.35	3.51	5.34	16.97	0.34	5.23	3.27	−1.48	10.28
DU-145	39.88	−4.79	2.24	−10.34	−5.92	9.02	−9.30	55.69	−5.96	4.21	−5.32	1.80

Table 3 (continued)

Subpanel/cancer cell lines	Growth inhibition percentage (GI%)											
	7a	7b	7c	7d	8	10	11	12a	12b	12c	12d	12e
Breast cancer												
MCF7	60.26	27.15	14.49	8.93	5.97	-2.27	1.64	92.05	10.67	8.54	1.59	13.23
MDA-MB-231/ATCC	30.16	19.53	13.48	7.67	-2.11	22.18	7.82	23.18	39.20	0.50	14.92	39.27
HS 578T	44.58	28.63	26.42	5.33	-3.54	-3.93	12.74	4.15	26.79	17.25	18.13	23.89
BT-549	33.87	13.54	-1.33	5.07	2.02	5.06	-4.06	-3.12	-5.02	-3.36	4.02	8.95
T-47D	35.70	42.61	23.11	14.72	2.16	24.47	9.08	11.45	15.46	4.54	12.39	19.51
MDA-MB-468	13.65	0.80	13.67	6.06	-11.53	-0.69	-10.77	-13.58	0.17	-30.88	10.89	11.35
MEAN% GI	29.40	10.56	10.23	-0.38	-1.90	-2.34	-3.99	9.99	6.17	2.65	5.63	9.10

NA; not available.

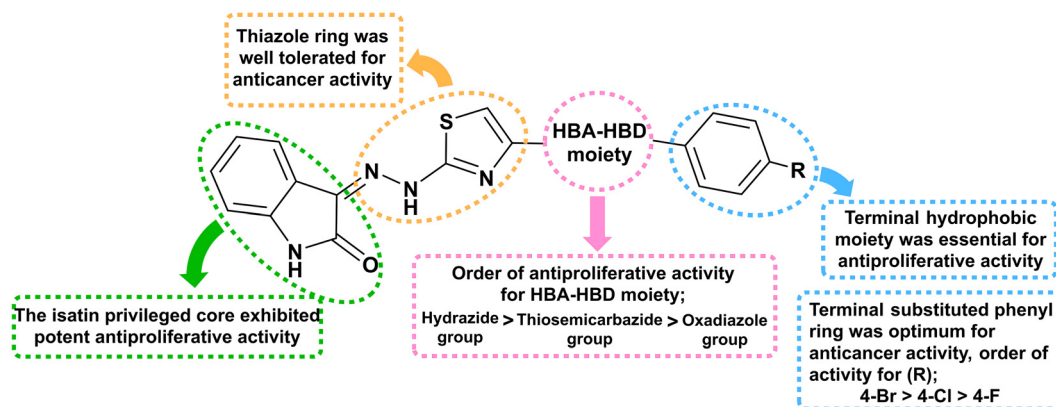


Fig. 4 Structure-anticancer activity relationship of the synthesized 2-oxoindolin-3-ylidene thiazole derivatives.

compound **4c** is a promising candidate for anticancer development.

2.2.4. Cell cycle analysis. Compound **4c**, which displayed remarkable cytotoxic potency and significant inhibitory activity against VEGFR-2, was selected for mechanistic investigation of its effect on cell cycle development and apoptosis induction in HepG2 cells. HepG2 cells were treated with compound **4c** at a concentration of 5.67 μM (IC_{50} value) for 24 hours, followed by flow cytometry analysis to compare cell cycle distribution with control cells. The results summarized in Table 7, showed a significant increase in the percentage of cells arrested in the G0/G1 phase, rising from 46.02% in control cells to 66.93% in treated cells. Furthermore, the percentage of cells in the S phase decreased from 36.57% in control cells to 10.65% in treated cells, suggesting a reduced rate of DNA synthesis, further supporting the hypothesis of cell cycle arrest. Additionally, the percentage of cells in the G2/M phase increased from 17.41% in control cells to 22.42% in treated cells. These findings demonstrate that compound **4c** induces cell cycle arrest in HepG2 cells mainly at the G0/G1 phase (Fig. 5).

2.2.5. Apoptosis analysis. The apoptotic activity of compound **4c** was investigated using an annexin-V/propidium iodide (PI) staining assay, which differentiates between living, early apoptotic, late apoptotic, and necrotic cells. HepG2 cells were treated with compound **4c** at its IC_{50} concentration

(5.67 μM) for 24 hours. The results revealed that compound **4c** significantly increased apoptosis compared to control cells, as reported in Table 8. Specifically, early apoptosis (lower right quadrant) increased from 0.55% in control cells to 15.26% in treated cells. Moreover, late apoptosis (upper right quadrant) showed a remarkable 76-fold increase, rising from 0.13% in control cells to 9.94% in treated cells. Additionally, compound **4c** also enhanced the percentage of necrotic cells by 1.72 times compared to the control (Fig. 6).

2.2.6. Caspase-3 and -9 expression assay. The sequential activation of caspases plays a crucial role in the process of cellular apoptosis.⁵⁹ Caspases are classified into two categories: initiators, such as caspase-9, which are involved early in the apoptotic cascade, and effectors, like caspase-3, which are activated by the initiators to execute cell death.⁶⁰ To explore the apoptotic mechanism of compound **4c**, the gene expression fold change of caspase-3 and -9 in HepG2 cells treated with 5.67 μM of the compound for 24 hours was analysed using quantitative real-time PCR. Notably, compound **4c** significantly upregulated the expression of caspase-3 and -9 by 6.50-fold and 2.99-fold, respectively compared to control cells (Fig. 7), suggesting that compound **4c** induces apoptosis through a caspase-dependent pathway.

2.2.7. In vitro wound healing assay. Cell migration plays a crucial role in angiogenesis, particularly during the early stages of the angiogenic cascade.⁶¹ VEGF, a proangiogenic

Table 4 *In vitro* NCI cell lines anticancer screening results of compounds **4b**, **4c**, **4d**, **4l**, and **6c** at five dose concentration reported in μM

Subpanel/cancer cell lines	4b GI ₅₀	4c GI ₅₀	4d GI ₅₀	4l GI ₅₀	6c GI ₅₀
Leukemia					
CCRF-CEM	17.30	5.35	9.14	8.31	2.93
HL-60(TB)	12.90	43.10	23.40	12.50	6.29
K-562	4.14	5.10	9.92	3.68	3.39
MOLT-4	6.97	4.09	9.19	4.61	11.00
RPMI-8226	6.16	6.40	6.91	5.21	14.80
SR	3.75	NA	NA	2.46	2.70
Non-small cell lung cancer					
A549/ATCC	2.13	1.75	23.60	4.00	11.20
EKVX	2.44	2.43	18.20	4.38	10.20
HOP-62	2.59	2.17	19.40	8.43	6.74
HOP-92	2.59	2.00	15.50	10.80	2.26
NCI-H226	2.69	3.13	20.20	11.90	5.54
NCI-H23	2.30	1.98	15.50	7.30	7.84
NCI-H322M	7.23	3.78	27.80	19.60	11.60
NCI-H460	2.00	2.05	27.90	3.65	6.11
NCI-H522	4.57	2.56	15.60	16.20	7.55
Colon cancer					
COLO 205	3.50	2.00	19.20	8.56	15.90
HCC-2998	2.76	3.05	15.80	6.18	10.70
HCT-116	3.08	3.26	19.20	3.57	11.20
HCT-15	3.04	2.44	11.40	3.65	5.50
HT 29	2.37	2.14	17.40	2.36	16.40
KM12	3.46	3.64	18.50	13.90	10.80
SW-620	2.06	2.33	18.80	3.35	11.80
CNS cancer					
SF-268	2.95	4.03	21.40	9.23	7.78
SF-295	2.15	1.71	14.30	9.36	4.12
SF-539	2.22	NA	NA	5.18	3.91
SNB-19	2.48	2.25	17.00	4.01	6.47
SNB-75	1.88	2.33	14.10	3.20	1.67
U251	2.03	1.74	14.00	2.92	5.53
Melanoma					
LOX IMVI	2.04	1.81	23.20	2.79	9.89
MALME-3M	4.29	2.73	12.80	9.83	12.00
M14	5.01	3.24	22.60	6.18	10.80
MDA-MB-435	3.81	3.79	16.90	7.30	11.70
SK-MEL-2	2.99	2.54	14.90	13.80	10.70
SK-MEL-28	3.35	1.93	15.50	8.95	11.30
SK-MEL-5	2.81	2.79	14.10	4.71	5.22
UACC-257	4.62	3.55	16.80	4.08	15.00
UACC-62	3.65	3.55	19.70	13.00	5.26
Ovarian cancer					
IGROV1	2.67	2.30	17.90	10.40	12.50
OVCAR-3	2.09	2.11	17.10	10.00	10.80
OVCAR-4	2.41	2.63	11.40	4.69	14.20
OVCAR-5	2.93	2.06	14.60	10.30	13.50
OVCAR-8	2.43	2.70	11.10	4.95	10.90
NCI/ADR-RES	2.09	1.99	5.02	2.77	16.30
SK-OV-3	2.95	3.61	30.20	11.50	13.20
Renal cancer					
786-0	1.69	1.89	18.00	2.82	13.30
A498	2.34	5.88	20.40	14.60	13.80
ACHN	2.59	2.47	14.60	8.57	9.72
CAKI-1	2.27	2.57	12.10	15.10	5.41
RXF 393	2.02	1.79	3.27	2.79	2.17
SN12C	2.29	2.30	13.10	5.92	11.80
TK-10	2.91	3.08	16.20	6.16	10.40
UO-31	3.24	2.24	14.40	11.10	5.58
Prostate cancer					
PC-3	3.06	3.46	16.30	9.07	10.30
DU-145	2.23	2.25	15.50	5.18	14.90

Table 4 (continued)

Subpanel/cancer cell lines	4b GI ₅₀	4c GI ₅₀	4d GI ₅₀	4l GI ₅₀	6c GI ₅₀
Breast cancer					
MCF7	2.48	2.57	8.97	2.54	12.20
MDA-MB-231/ATCC	2.22	1.96	17.30	2.92	12.80
HS 578T	2.55	2.61	18.40	3.57	2.94
BT-549	2.51	2.23	9.74	6.63	5.91
T-47D	2.26	2.86	12.90	3.48	6.78
MDA-MB-468	1.86	2.42	13.90	2.97	13.30
MG-MID^a	2.95	2.82	15.14	6.03	8.13

^a GI₅₀ (μM) full panel mean-graph midpoint (MG-MID) = the average sensitivity of all cell lines toward the target compounds. NA; not available.

factor, stimulates proliferation, migration, and tube formation in HepG2 cells. To evaluate cancer cell migration *in vitro*, the wound healing (scratch or migration) assay is commonly used. In this assay, a scratch was created in a monolayer of HepG2 cancer cells, and the initial gap width was measured. The closure of the scratch was monitored over 0 to 72 hours in both **4c**-treated and untreated cells (Fig. 8). The results (Table 9) demonstrated that the scratch in the untreated HepG2 control cells closed significantly within 72 hours, achieving a closure rate of 98.52%. In contrast, **4c**-treated HepG2 cells showed a reduction in wound closure to 60.74%, demonstrating that compound **4c** effectively inhibited cell migration and delayed wound closure.

2.3. Molecular modeling studies

2.3.1. Docking study. The molecular docking study was performed to predict the possible binding mode and interactions of the target compounds within the active binding site of VEGFR-2. Sunitinib was considered a reference drug in that study. The docking simulations were performed using MOE (Molecular Operating Environment, version 2020.09 computational software, Chemical Computing Group Inc., Canada) software to predict the

Table 5 Cytotoxicity represented by IC₅₀ μM for the most potent compounds **4b**, **4c**, **4d**, **4l**, **6c**, and sunitinib against hepatic cancer cell line (HepG2) and normal liver cell line (THLE-2) with values of selectivity index (SI)^b

Compound	(IC ₅₀ , ^a μM)		SI ^b
	HepG2	THLE-2	
4b	21.98 \pm 0.72	39.64 \pm 1.46	1.80
4c	5.67 \pm 0.19	44.70 \pm 1.94	7.88
4d	11.62 \pm 0.38	40.61 \pm 1.77	3.49
4l	30.54 \pm 1.01	108.96 \pm 4.6	3.57
6c	3.13 \pm 0.1	32.06 \pm 1.18	10.26
Sunitinib	23.44 \pm 0.77	26.90 \pm 0.99	1.15

^a IC₅₀ values are the mean \pm SD of three separate experiments. ^b SI: the ratio of IC₅₀ against THLE-2 normal cells to IC₅₀ against HepG2 tumor cell lines, respectively. All measurements were done in triplicate.

Table 6 *In vitro* VEGFR-2 kinase inhibitory activities of compounds **4b**, **4c**, **4d**, **4l**, **6c**, and sunitinib

Compound	(IC ₅₀ , ^a μM)
4b	0.113 ± 0.005
4c	0.047 ± 0.002
4d	1.549 ± 0.063
4l	0.995 ± 0.04
6c	0.089 ± 0.004
Sunitinib	0.167 ± 0.007

^a All IC₅₀ values are calculated as the mean ± SD of three different experiments.

Table 7 The effect of **4c** on cell cycle distribution in the HepG2 cells

Sample	Cell cycle distribution		
	% G0/G1	% S	% G2/M
Control HepG2	46.02	36.57	17.41
4c /HepG2	66.93	10.65	22.42

affinity and investigate the potential binding pattern of target compounds **2–12a–e** within the active site of VEGFR-2 tyrosine kinase co-crystallized with sunitinib (PDB: 4AGD).⁶² Sunitinib (docking score = −8.5155 kcal mol^{−1}) displayed H-bond interactions by the NH and C=O groups of its indolin-2-one with Glu917 and Cys919 of hinge residues, respectively. Additionally, it showed multiple hydrophobic interactions with Leu840, Val848, Gly922, and Phe1047 (Fig. 9). The synthesized compounds showed similar binding mode and orientation to sunitinib inside the active binding site of VEGFR-2 with docking scores ranging from −6.8036 to −9.3962 kcal mol^{−1}, as reported in the ESI† (Table S6).

The docking simulations of compounds **4b**, **4c**, and **6c** within the ATP binding pocket of VEGFR-2 (Fig. 9 and 10) showed effective fitting into the hinge region, aligning similarly to sunitinib. The results of the docking study were reported in Table 10. Each derivative demonstrated two critical hydrogen bond interactions: the NH and C=O groups

Table 8 The effect of **4c** on apoptosis in the HepG2 cells

Sample	Apoptosis		Necrosis
	Early	Late	
Control HepG2	0.55	0.13	1.58
4c /HepG2	15.26	9.94	2.72

of their indolin-2-one scaffold interacted with the Glu917 and Cys919 hinge residues, respectively. Additionally, various hydrophobic and Van der Waals interactions with Leu840, Val848, and Phe1047 further stabilized the binding. The halogenated derivatives **4b** and **4c** exhibited halogen bond interactions between their halogen atoms and the Asp1052 residue, which likely enhanced their binding affinity and contributed to their increased inhibitory activity against VEGFR-2. For **4b** and **4c**, the halogen bond lengths and angles are 3.23 Å, 149.2° and 3.35 Å, 157.0°, respectively. The bond distances are lower than the sum of the respective Van der Waals radii of atoms, indicating that there is an attractive chemical force between the atoms. Compound **4c** also showed a chalcogen bond interaction between sulfur atom of the thiazole ring and Cys919 residue. Finally, compound **6c** exhibited two H-bonds by sulfur atom of thiosemicarbazide linker with Arg1051 and Gly841 residues.

The molecular docking study highlighted the ability of these compounds to interact with key amino acids within the ATP binding site of VEGFR-2. The observed binding interactions and docking scores strongly correlate with the experimental *in vitro* anticancer activity and VEGFR-2 kinase inhibition results, supporting the potential of these compounds as effective antitumor agents.

2.3.2. *In silico* physicochemical and pharmacokinetic properties prediction. Evaluating the physicochemical and pharmacokinetic parameters of newly designed compounds is crucial in the early stages of drug discovery to ensure the development of viable drug candidates.⁶³ In this study, *in silico* investigation of the pharmacokinetic properties and drug-likeness of the synthesized compounds was investigated

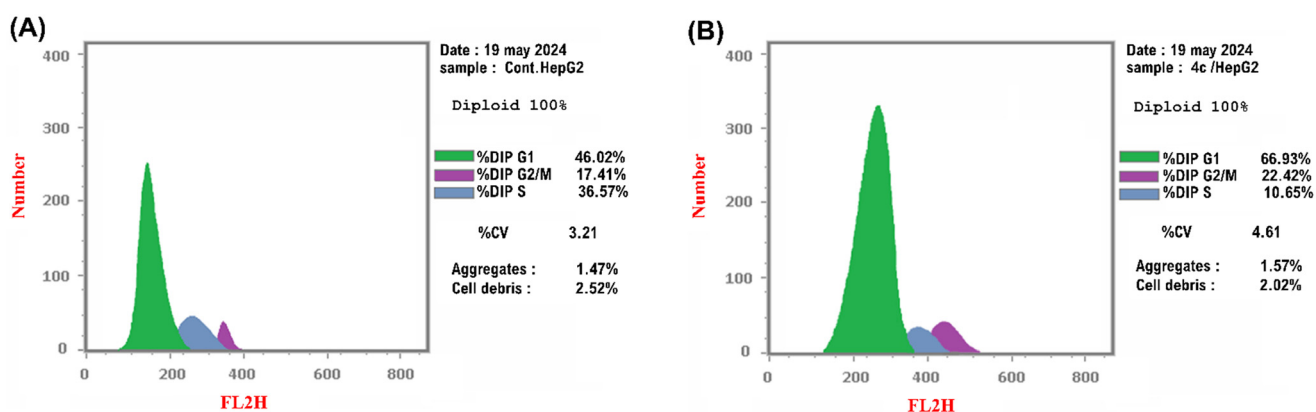


Fig. 5 Cell cycle analysis of the HepG2 cells treated with **4c** for 24 h using flow cytometry. (A) Control cells and (B) **4c**-treated cells. Compound **4c** induced cell cycle arrest in HepG2 cells at the G0/G1 phase (66.93%) in comparison to control cells (46.02%).

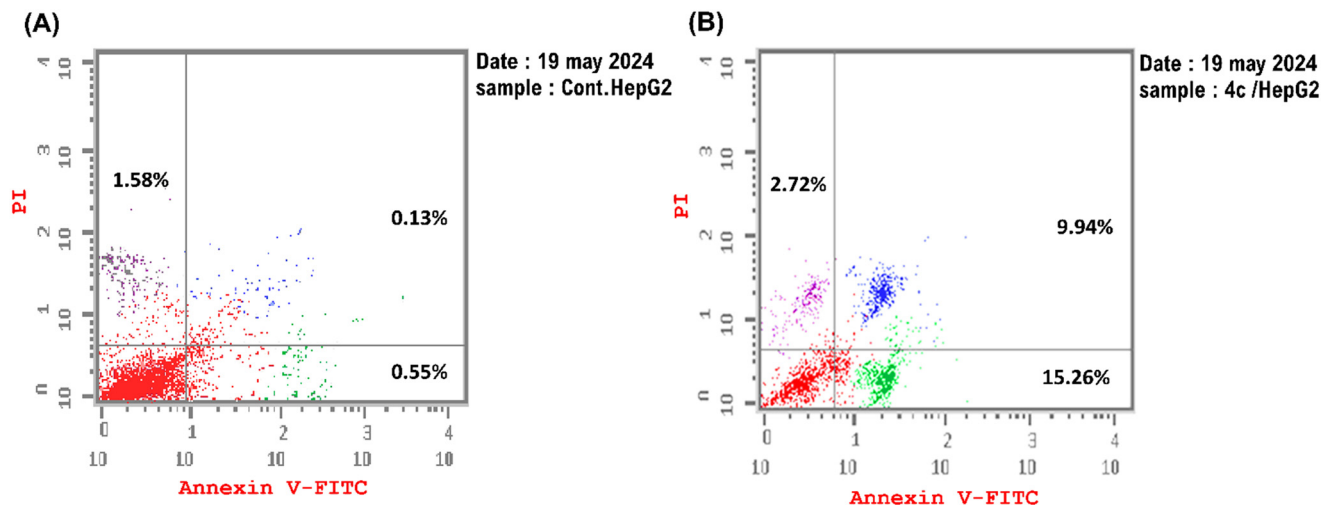


Fig. 6 The effect of **4c** on apoptosis in the HepG2 cells using annexin V-FITC/PI dual staining. (A) Control cells and (B) **4c**-treated cells. Compound **4c** increased the early and late apoptosis from 0.55% and 0.13% in control cells to 15.26% and 9.94% in **4c**-treated cells.

using the SwissADME tool provided by the Swiss Institute of Bioinformatics (<http://www.swissadme.ch/index.php>).⁶⁴

The oral bioavailability of compounds **4b**, **4c**, **4d**, **4l**, and **6c** was assessed using Lipinski and Veber rules, with sunitinib as a reference. The predicted parameters were summarized in Table 11. The molecular weights of the compounds ranged from 408.41 to 451.52 g mol⁻¹, with MLOG P values between 1.56 and 2.05, whereas sunitinib had molecular weight of 398.47 g mol⁻¹ and MLOG P value of 2.06. The hydrogen bond acceptors (HAs) and hydrogen bond donors (HDs) for the compounds varied from 4 to 6 and 3 to 5, respectively, compared to sunitinib's values of 4 and 3. Additionally, the topological polar surface area (TPSA) of compounds ranged from 136.08 Å² to 179.87 Å². The number of rotatable bonds (RBs) for both the compounds and sunitinib ranged from 6 to 8. Overall, the results indicated

that compounds **4b**, **4c**, **4d**, and **4l** comply with Lipinski and Veber rules, similar to sunitinib. Their potent cytotoxic activity, combined with favourable drug-likeness and pharmacokinetic properties, suggests they could be promising candidates for further drug development.

2.3.3. Quantum chemistry calculations. An essential aspect influencing drug reactivity is the examination of frontier molecular orbitals (FMOs). These orbitals provide insights into several reactivity descriptors, such as ionization potential (IP), electron affinity (EA), electronegativity (χ), chemical potential (μ), global hardness (η), global softness (S), and electrophilicity index (ω), calculated using equations from Koopman's theory.⁶⁵ The global quantum descriptors, along with the dipole moment (Dm) and total ground state energy (E_T), are summarized in Table 12.

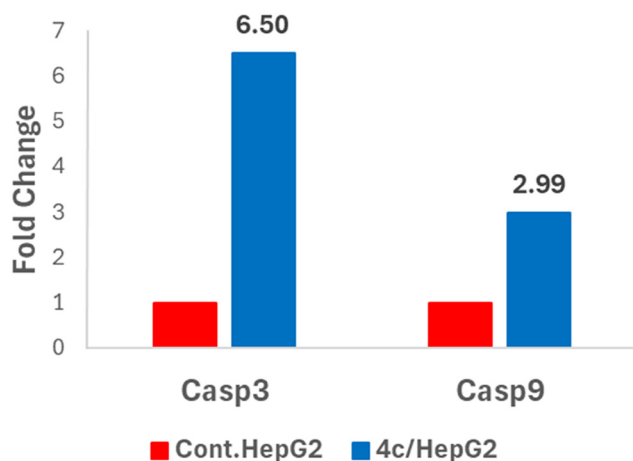


Fig. 7 The gene expression fold change of caspases-3 and -9 in HepG2 cells treated with **4c**. Compound **4c** significantly increased the expression of caspase-3 and -9 by 6.50-fold and 2.99-fold in comparison to control cells.

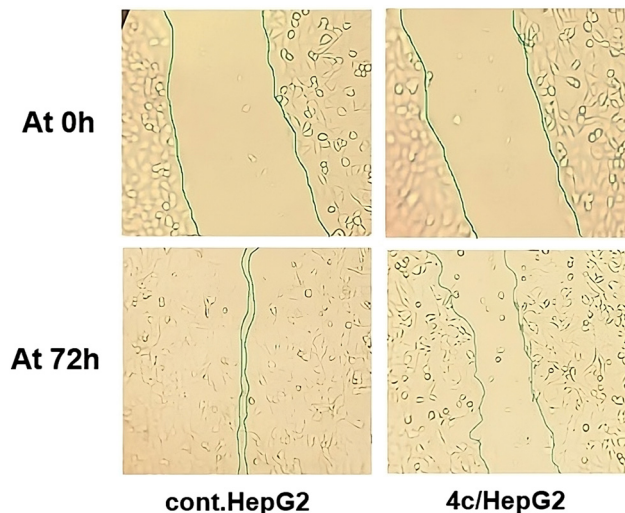
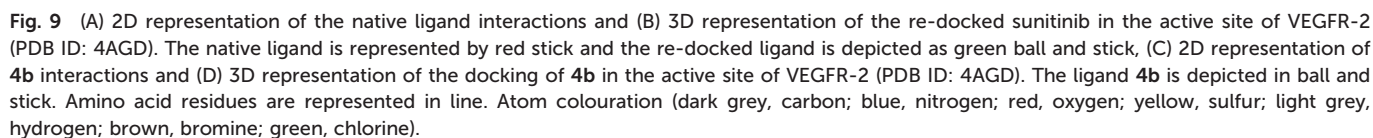


Fig. 8 The effect of **4c** on migration and healing of HepG2 cells. Compound **4c** delayed the wound closure by 60.74%.

	Wound area at 0 h (μm^2)	Wound area at 72 h (μm^2)	Wound closure %
Untreated HepG2 cells	228	3.37	98.52
4c -treated HepG2 cells	225	88.33	60.74



2.3.4. The electron density map. The reactivity potential of compound **4c** can be evaluated through DFT calculations. The total electron density (TED) map (Fig. 12) displayed the electron distribution across the molecule. The electron density map of **4c** aligns with the orientation and interactions within the VEGFR-2 active site. The red region

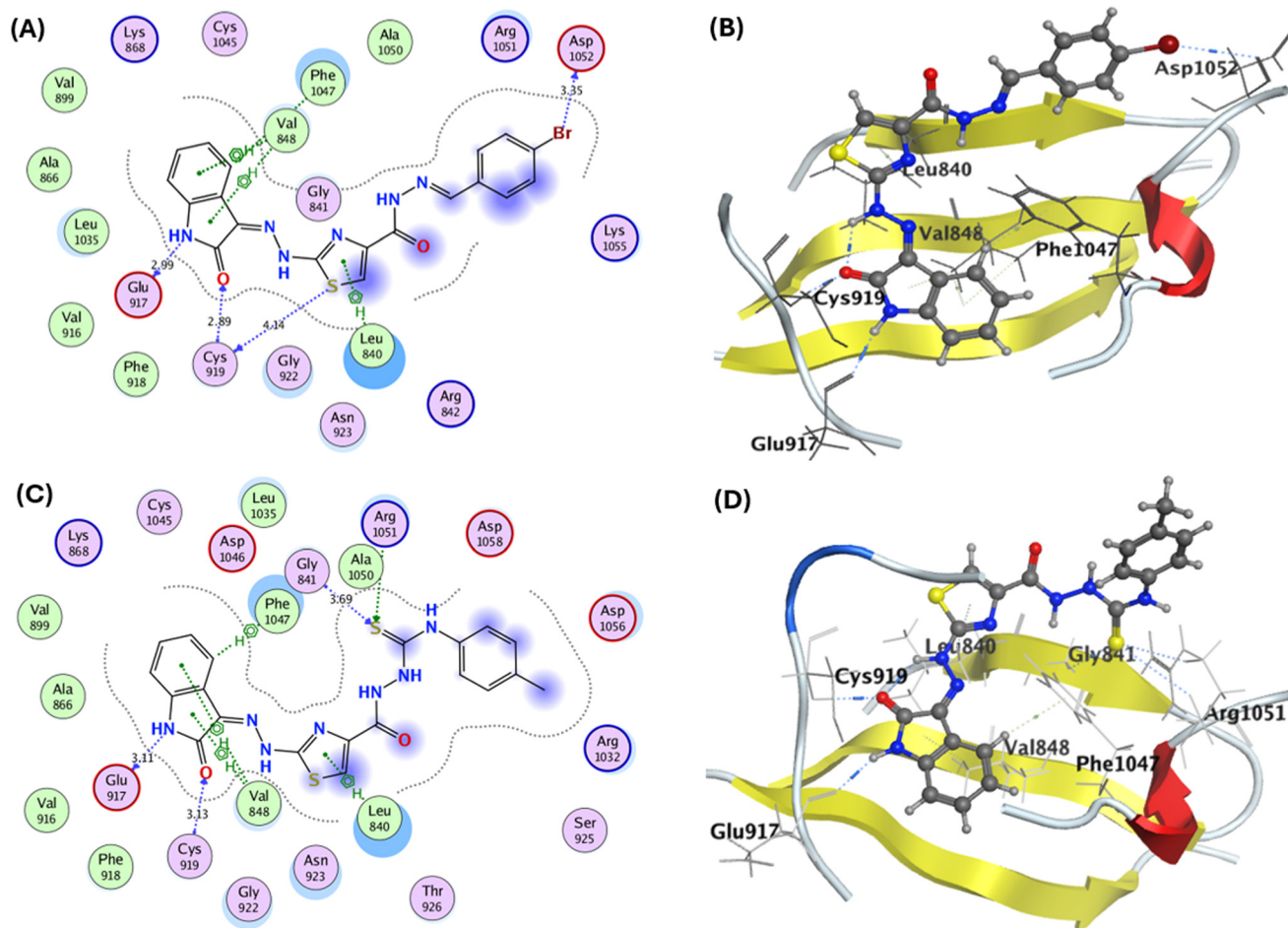


Fig. 10 (A) 2D representation of **4c** interactions and (B) 3D representation of the docking of **4c** in the active site of VEGFR-2 (PDB ID: 4AGD), (C) 2D representation of **6c** interactions and (D) 3D representation of the docking of **6c** in the active site of VEGFR-2 (PDB ID: 4AGD). The ligands **4c** and **6c** are depicted in ball and stick. Amino acid residues are represented in line. Atom colouration (dark grey, carbon; blue, nitrogen; red, oxygen; yellow, sulfur; light grey, hydrogen; brown, bromine; green, chlorine).

highlights the electronegative atoms, revealing the nucleophilic attack of the O atom of indolin-2-one onto the amino acid (Cys919). The yellow and green regions have moderate electronegativity, indicating possible hydrophobic interactions. The moieties of indolin-2-one and thiazole were attracted by amino acids (Leu840, Val848, and Phe1047). Meanwhile, the blue region represents the most favorable electropositive atoms, which explains the nucleophilic attack of amino acid (Glu917) onto the NH atoms of indolin-2-one.⁶⁷

3. Materials and methods

3.1. Chemistry

All chemicals and solvents used for synthesis of the targeted compounds were purchased from commercial sources and were of the highest pure form. Reactions were monitored by thin layer chromatography (TLC) using precoated aluminium sheets, silica gel Kieselgel 60G F254 (Merck, Darmstadt, Germany). TLC sheets were visualized using UV lamp at 254 nm. Silica gel (100–200 mesh) was used for column

chromatography. Melting points were determined in °C using Stuart electrothermal melting point apparatus (Stuart Scientific, UK) and were uncorrected. Infrared spectra were recorded as KBr discs using Thermo Scientific Nicolet iS10 FT-IR spectrometer, Faculty of Science, Assiut University, Assiut, Egypt, and the results were presented as cm^{-1} . NMR spectra were performed on Bruker Avance III HD FT-high resolution NMR Spectrophotometer (400 MHz for ^1H and 100 MHz for ^{13}C), Faculty of Pharmacy, Mansoura University, Mansoura, Egypt, as well as on Bruker Magnet System 400/54 Ascend/R NMR Spectrophotometer (400 MHz for ^1H and 100 MHz for ^{13}C), Faculty of Science, Zagazig University, Zagazig, Egypt (the ESI† Fig. S1–S36). Chemical shifts are expressed in δ values (ppm) relative to the internal standard tetramethylsilane (TMS) at δ 0.00 ppm and are referenced relative to residual solvent (e.g., DMSO- d_6 : δ H = 2.50 ppm in ^1H NMR, C = 39.5 ppm in ^{13}C NMR). Coupling constants (J) were given in hertz (Hz) and expressed as s, singlet; d, doublet; t, triplet; q, quartet; m, multiplet. Elemental analysis was performed on Thermo Scientific Flash 2000 CHNS/O analyzer, at the regional center for Mycology and

Table 10 The binding interactions, distances, angles, docking scores, and root mean square deviation of compounds **4b**, **4c**, **6c**, and sunitinib

Compound no.	Amino acid residues/type of interactions	Distance Å	Angle °	Score kcal mol ⁻¹	rmsd_refine Å
4b	Glu917/H-bond	2.99	159.7	-9.0071	0.4084
	Cys919/H-bond	2.96	171.1		
	Asp1052/halogen bond	3.23	149.2		
	Phe1047/H- π	3.94	147.2		
	Leu840/ π -H	4.24	177.9		
	Val848/ π -H	4.23	158.7		
	Val848/ π -H	4.32	152.9		
4c	Glu917/H-bond	2.99	157.8	-9.3962	0.5178
	Cys919/H-bond	2.89	171.3		
	Cys919/chalcogen bond	4.14	149.9		
	Asp1052/halogen bond	3.35	157.0		
	Phe1047/H- π	3.91	142.6		
	Leu840/ π -H	4.19	175.4		
	Val848/ π -H	4.29	157.4		
	Val848/ π -H	4.33	155.6		
	Glu917/H-bond	3.11	154.6		
6c	Cys919/H-bond	3.13	169.0	-8.8212	0.6037
	Gly841/H-bond	3.69	127.1		
	Arg1051/H-bond	4.71	146.9		
	Phe1047/H- π	4.00	154.7		
	Leu840/ π -H	4.19	165.0		
	Val848/ π -H	4.23	161.0		
	Val848/ π -H	4.37	151.0		
	Glu917/H-bond	3.02	151.7		
	Cys919/H-bond	2.98	175.9		
Sunitinib	Phe1047/H- π	4.11	150.8	-8.5155	0.9625
	Leu840/ π -H	4.05	152.7		
	Val848/ π -H	4.29	157.2		
	Val848/ π -H	4.30	153.7		
	Gly922/ π -H	3.54	130.1		

Table 11 Calculated physicochemical and pharmacokinetic parameters of compounds **4b**, **4c**, **4d**, **4l**, **6c**, and sunitinib

Compound	MW (g mol ⁻¹)	HAs	HDs	log $P_{o/w}$ (MLOG P)	Lipinski violations	TPSA (Å ²)	RBs	Veber violations
4b	424.86	5	3	1.93	0	136.08	6	0
4c	469.31	5	3	2.05	0	136.08	6	0
4d	408.41	6	3	1.82	0	136.08	6	0
4l	416.46	5	3	1.82	0	136.08	7	0
6c	451.52	4	5	1.56	0	179.87	8	1
Sunitinib	398.47	4	3	2.06	0	77.23	8	0

Table 12 The DFT global reactivity parameters for compound **4c**

IP	EA	χ (eV)	μ (eV)	η (eV)	S (eV)	ω (eV)	Dm (Debye)	E_T (a.u.)
5.8490	2.6885	4.2688	-4.2688	1.5803	0.6328	5.7656	10.0119	-4162.1233

Biotechnology, Al-Azhar University, Cairo, Egypt, and the result values were within $\pm 0.4\%$ of the theoretical values. Mass spectrum was carried out on direct inlet part to mass analyzer in Thermo Scientific GCMS model ISQ at the regional center for Mycology and Biotechnology, Al-Azhar University, Cairo, Egypt. Substituted phenacyl bromides **9a–c** were prepared according to the reported procedures.^{68,69} The final compounds were obtained as a mixture of *E* and *Z* isomers. The ratio was determined from ¹H NMR, and the spectral data were reported for the major isomer.

3.1.1. Synthesis of (Z)-2-(2-oxoindolin-3-ylidene)hydrazine-1-carbothioamide **1** was prepared according to the reported procedure described in ref. 40. Yellow solid; yield 0.69 g (92%); mp 260–262 °C (lit. 40 mp 254 °C).

3.1.2. Synthesis of ethyl (Z)-2-[2-(2-oxoindolin-3-ylidene)hydrazineyl]thiazole-4-carboxylate **2**. Ethyl bromopyruvate (0.35 mL, 2.27 mmol) was added to a solution of **1** (0.5 g, 2.27 mmol) in absolute ethanol (15 mL), and the mixture was refluxed for 12 h. After cooling to room temperature, the precipitate was filtered, dried, and recrystallized from methanol.

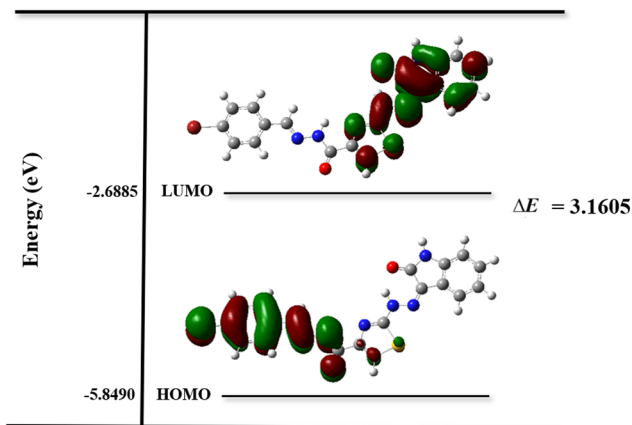


Fig. 11 Energy gap (ΔE), frontier molecular orbitals; HOMO and LUMO at the ground state for compound **4c**.

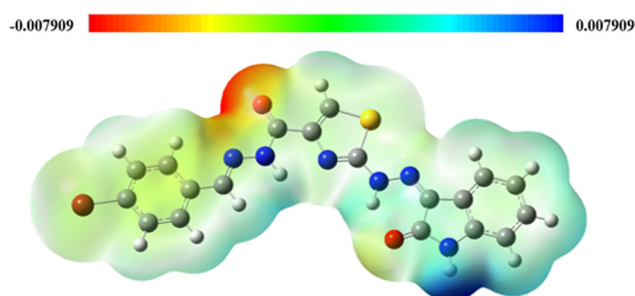


Fig. 12 Total electron density map of the target compound **4c**.

Yellow solid; yield 0.64 g (90%); mp 249–251 °C; FT-IR: 3436, 3186, 3123, 1716, 1680, 1655, 1618, 1551, 1463; ^1H NMR: 13.28 (s, 1H), 11.24 (s, 1H), 8.04 (s, 1H), 7.54 (d, J = 8 Hz, 1H), 7.35 (t, J = 8 Hz, 1H), 7.09 (t, J = 8 Hz, 1H), 6.97 (d, J = 8 Hz, 1H), 4.28 (q, J = 7.1 Hz, 2H), 1.30 (t, J = 7 Hz, 3H); ^{13}C NMR: 166.8, 163.5, 161.1, 143.5, 142.0, 133.4, 131.3, 122.9, 122.5, 120.5, 120.1, 111.6, 61.2, 14.6; ESI-MS m/z : 316.39 [M^+]; anal. calcd. for $\text{C}_{14}\text{H}_{12}\text{N}_4\text{O}_3\text{S}$: C, 53.16; H, 3.82; N, 17.71; S, 10.14. Found: C, 53.40; H, 3.98; N, 17.99; S, 10.27.

3.1.3. Synthesis of (Z/E)-2-[2-(2-oxoindolin-3-ylidene)hydrazineyl]thiazole-4-carbohydrazide 3. To a mixture of **2** (0.2 g, 0.63 mmol), hydrazine hydrate (0.47 g, 9.49 mmol, d = 1.032 g mL $^{-1}$) was added in absolute ethanol (10 mL). The mixture was refluxed for 24 h. After cooling to room temperature, the precipitate was filtered, dried, and recrystallized from ethanol.

Orange solid; yield 0.18 g (95%); mp 290–293 °C; FT-IR: 3340, 3323, 3237, 1682, 1665, 1622, 1586, 1458, 1439, 1198; ^1H NMR: 11.24 (s, 1H), 9.60 (s, 1H), 7.74 (s, 1H), 7.53 (d, J = 8 Hz, 1H), 7.34 (t, J = 8 Hz, 1H), 7.09 (t, J = 6 Hz, 1H), 6.96 (d, J = 8 Hz, 1H); ^{13}C NMR: 166.6, 163.6, 160.1, 146.1, 141.9, 133.2, 131.2, 123.0, 120.5, 120.1, 116.5, 111.6; ESI-MS m/z : 302.34 [M^+]; anal. calcd. for $\text{C}_{12}\text{H}_{10}\text{N}_6\text{O}_2\text{S}$: C, 47.68; H, 3.33; N, 27.80; S, 10.61. Found: C, 47.93; H, 3.45; N, 27.67; S, 10.68.

3.1.4. General procedure for the synthesis of compounds 4a–o. A mixture of substituted aromatic aldehyde or ketone (0.66 mmol) was added to a solution of **3** (0.2 g, 0.66 mmol),

and 0.2 mL glacial acetic acid in absolute ethanol (15 mL) was refluxed for the specified time (18–30 h). After cooling to room temperature, the precipitate was filtered and dried. The precipitate was triturated several times with diethyl ether and filtered to yield **4a–o** (70–90%).

***N'*-(*E*-Benzylidene)-2-[2-((*Z*)-2-oxoindolin-3-ylidene)hydrazineyl]thiazole-4-carbohydrazide 4a.** Yellow solid; yield 0.23 g (88%); mp >300 °C; FT-IR: 3302, 3250, 1701, 1681, 1622, 1558, 1545, 1488, 1469, 1156; ^1H NMR: 13.37 (s, 1H), 11.83 (s, 1H), 11.27 (s, 1H), 8.58 (s, 1H), 7.97 (s, 1H), 7.71 (d, J = 8 Hz, 2H), 7.56 (d, J = 8 Hz, 1H), 7.50–7.44 (m, J = Hz, 3H), 7.36 (t, J = 8 Hz, 1H), 7.11 (t, J = 6 Hz, 1H), 6.97 (d, J = 8 Hz, 1H); ^{13}C NMR: 168.1, 166.8, 163.7, 157.3, 149.0, 145.9, 142.0, 134.8, 133.5, 131.4, 130.6, 129.3, 127.6, 123.0, 120.6, 118.8, 111.6; anal. calcd. for $\text{C}_{19}\text{H}_{14}\text{N}_6\text{O}_2\text{S}$: C, 58.45; H, 3.61; N, 21.53; S, 8.21. Found: C, 58.74; H, 3.75; N, 21.80; S, 8.34.

***N'*-(*E*-4-Chlorobenzylidene)-2-[2-((*Z*)-2-oxoindolin-3-ylidene)hydrazineyl]thiazole-4-carbohydrazide 4b.** Yellow solid; yield 0.22 g (79%); mp 263–265 °C; FT-IR: 3342, 3253, 1694, 1674, 1620, 1557, 1488, 1468, 1163; ^1H NMR: 13.38 (s, 1H), 11.91 (s, 1H), 11.27 (s, 1H), 8.56 (s, 1H), 7.98 (s, 1H), 7.72 (d, J = 8 Hz, 2H), 7.57 (d, J = 8 Hz, 1H), 7.53 (d, J = 8 Hz, 2H), 7.36 (td, J = 8, 4 Hz, 1H), 7.11 (t, J = 8 Hz, 1H), 6.98 (d, J = 8 Hz, 1H); ^{13}C NMR: 166.2, 163.2, 156.8, 147.1, 145.3, 141.5, 134.5, 133.3, 133.0, 130.8, 128.9, 128.7, 122.5, 120.1, 119.5, 118.4, 111.1; ESI-MS m/z : 424.78 [M^+]; anal. calcd. for $\text{C}_{19}\text{H}_{13}\text{ClN}_6\text{O}_2\text{S}$: C, 53.71; H, 3.08; N, 19.78; S, 7.55. Found: C, 53.94; H, 3.17; N, 20.04; S, 7.69.

***N'*-(*E/Z*-4-Bromobenzylidene)-2-[2-((*Z*)-2-oxoindolin-3-ylidene)hydrazineyl]thiazole-4-carbohydrazide 4c.** Yellow solid; yield 0.28 g (90%); mp 284–286 °C; FT-IR: 3554, 3407, 3282, 1682, 1616, 1558, 1486, 1468, 1167; ^1H NMR: 13.37 (s, 1H), 11.91 (s, 1H), 11.27 (s, 1H), 8.54 (s, 1H), 7.97 (s, 1H), 7.67–7.62 (m, 4H), 7.56 (d, J = 8 Hz, 1H), 7.36 (t, J = 8 Hz, 1H), 7.10 (t, J = 8 Hz, 1H), 6.97 (d, J = 8 Hz, 1H); ^{13}C NMR: 166.7, 163.7, 161.2, 157.3, 147.7, 145.8, 142.0, 134.1, 133.5, 133.4, 132.5, 132.3, 131.3, 130.7, 129.5, 125.5, 123.8, 123.0, 120.6, 120.0, 118.9, 111.6; ESI-MS m/z : 469.08 [M^+]; anal. calcd. for $\text{C}_{19}\text{H}_{13}\text{BrN}_6\text{O}_2\text{S}$: C, 48.62; H, 2.79; N, 17.91; S, 6.83. Found: C, 48.90; H, 3.01; N, 18.17; S, 6.94.

***N'*-(*E*-4-Fluorobenzylidene)-2-[2-((*Z*)-2-oxoindolin-3-ylidene)hydrazineyl]thiazole-4-carbohydrazide 4d.** Yellow solid; yield 0.19 g (70%); mp 297–300 °C; FT-IR: 3332, 3227, 1694, 1674, 1622, 1556, 1542, 1491, 1468, 1164; ^1H NMR: 13.35 (s, 1H), 11.83 (s, 1H), 11.26 (s, 1H), 8.55 (s, 1H), 7.95 (s, 1H), 7.76–7.73 (m, 2H), 7.55 (d, J = 4 Hz, 1H), 7.36 (t, J = 8 Hz, 1H), 7.29 (t, J = 8 Hz, 2H), 7.09 (t, J = 8 Hz, 1H), 6.96 (d, J = 8 Hz, 1H); ^{13}C NMR: 166.7, 163.7, 163.6 (d, J = 246 Hz), 157.3, 147.8, 145.9, 142.0, 133.5, 131.5 (d, J = 3 Hz), 129.8 (d, J = 9 Hz), 123.0, 120.6, 120.0, 118.8, 116.5 (d, J = 22 Hz), 111.6; ESI-MS m/z : 409.11 [M^+]; anal. calcd. for $\text{C}_{19}\text{H}_{13}\text{FN}_6\text{O}_2\text{S}$: C, 55.88; H, 3.21; N, 20.58; S, 7.85. Found: C, 56.04; H, 3.43; N, 20.84; S, 7.92.

***N'*-(*E*-4-Hydroxybenzylidene)-2-[2-((*Z*)-2-oxoindolin-3-ylidene)hydrazineyl]thiazole-4-carbohydrazide 4e.** Yellow solid; yield 0.19 g (70%); mp >300 °C; FT-IR: 3227, 1682, 1662,

1622, 1557, 1541, 1492, 1469, 1166; ^1H NMR: 11.62 (s, 1H), 11.26 (s, 1H), 9.94 (s, 1H), 8.45 (s, 1H), 7.92 (s, 1H), 7.56–7.52 (m, 3H), 7.35 (t, $J = 8$ Hz, 1H), 7.10 (t, $J = 8$ Hz, 1H), 6.97 (d, $J = 8$ Hz, 1H), 6.84 (d, $J = 8$ Hz, 2H); ^{13}C NMR: 166.7, 163.7, 159.9, 157.0, 149.3, 146.1, 142.0, 133.4, 131.3, 129.4, 125.8, 123.0, 120.6, 120.0, 118.3, 116.2, 111.6; anal. calcd. for $\text{C}_{19}\text{H}_{14}\text{N}_6\text{O}_3\text{S}$: C, 56.15; H, 3.47; N, 20.68; S, 7.89. Found: C, 56.41; H, 3.53; N, 20.89; S, 8.04.

N'-((*E*)-4-Methylbenzylidene)-2-[2-((*Z*)-2-oxoindolin-3-ylidene)hydrazineyl]thiazole-4-carbohydrazide **4f**. Yellow solid; yield 0.24 g (89%); mp 297–299 °C; FT-IR: 3541, 3417, 3314, 3120, 1682, 1617, 1556, 1495, 1164; ^1H NMR: 13.35 (s, 1H), 11.76 (s, 1H), 11.27 (s, 1H), 8.52 (s, 1H), 7.95 (s, 1H), 7.59 (d, $J = 8$ Hz, 2H), 7.55 (d, $J = 8$ Hz, 1H), 7.36 (t, $J = 8$ Hz, 1H), 7.27 (d, $J = 8$ Hz, 2H), 7.10 (t, $J = 8$ Hz, 1H), 6.97 (d, $J = 8$ Hz, 1H), 2.34 (s, 3H); ^{13}C NMR: 166.7, 163.7, 157.2, 149.0, 146.0, 142.0, 140.4, 133.5, 132.1, 131.3, 129.9, 127.6, 123.0, 120.6, 120.0, 118.7, 111.6, 21.5; anal. calcd. for $\text{C}_{20}\text{H}_{16}\text{N}_6\text{O}_2\text{S}$: C, 59.39; H, 3.99; N, 20.78; S, 7.93. Found: C, 59.57; H, 4.15; N, 20.92; S, 7.81.

N'-((*E/Z*)-4-Methoxybenzylidene)-2-[2-((*Z*)-2-oxoindolin-3-ylidene)hydrazineyl]thiazole-4-carbohydrazide **4g**. Yellow solid; yield 0.20 g (71%); mp 274–276 °C; FT-IR: 3253, 3121, 1684, 1622, 1563, 1551, 1501, 1170; ^1H NMR: 13.37 (s, 1H), 11.70 (s, 1H), 11.28 (s, 1H), 8.50 (s, 1H), 7.94 (s, 1H), 7.65 (d, $J = 8$ Hz, 2H), 7.57 (d, $J = 4$ Hz, 1H), 7.37 (td, $J = 8, 4$ Hz, 1H), 7.11 (d, $J = 8$ Hz, 1H), 7.03 (d, $J = 8$ Hz, 2H), 6.98 (d, $J = 8$ Hz, 1H), 3.82 (s, 3H); ^{13}C NMR: 160.4, 157.4, 155.8, 155.0, 154.6, 150.8, 142.5, 139.7, 135.7, 127.1, 125.0, 124.1, 122.9, 121.1, 120.7, 116.7, 114.3, 113.7, 112.2, 108.6, 108.5, 105.3, 49.5; anal. calcd. for $\text{C}_{20}\text{H}_{16}\text{N}_6\text{O}_3\text{S}$: C, 57.13; H, 3.84; N, 19.99; S, 7.63. Found: C, 57.40; H, 4.05; N, 20.17; S, 7.80.

N'-((*E*)-4-Hydroxy-3-methoxybenzylidene)-2-[2-((*Z*)-2-oxoindolin-3-ylidene)hydrazineyl]thiazole-4-carbohydrazide **4h**. Yellow solid; yield 0.23 g (79%); mp >300 °C; FT-IR: 3264, 3093, 1690, 1671, 1622, 1559, 1546, 1497, 1470, 1162; ^1H NMR: 11.65 (s, 1H), 11.26 (s, 1H), 9.58 (s, 1H), 8.44 (s, 1H), 7.92 (s, 1H), 7.54 (d, $J = 8$ Hz, 1H), 7.35 (t, $J = 8$ Hz, 1H), 7.31 (m, 1H), 7.10 (td, $J = 8, 4$ Hz, 1H), 7.05 (dd, $J = 8, 4$ Hz, 1H), 6.96 (d, $J = 8$ Hz, 1H), 6.85 (d, $J = 8$ Hz, 1H), 3.84 (s, 3H); ^{13}C NMR: 166.7, 163.7, 157.1, 149.5, 148.5, 146.1, 141.9, 133.4, 131.3, 126.2, 123.0, 122.8, 120.5, 120.0, 118.4, 115.9, 111.6, 109.4, 56.0; anal. calcd. for $\text{C}_{20}\text{H}_{16}\text{N}_6\text{O}_4\text{S}$: C, 55.04; H, 3.70; N, 19.26; S, 7.35. Found: C, 55.31; H, 3.62; N, 19.47; S, 7.49.

N'-((*E*)-3,4-Dimethoxybenzylidene)-2-[2-((*Z*)-2-oxoindolin-3-ylidene)hydrazineyl]thiazole-4-carbohydrazide **4i**. Yellow solid; yield 0.22 g (73%); mp 269–271 °C; FT-IR: 3447, 3326, 3270, 3115, 1699, 1670, 1622, 1558, 1490, 1469, 1152; ^1H NMR: 13.35 (s, 1H), 11.68 (s, 1H), 11.26 (s, 1H), 8.49 (s, 1H), 7.94 (s, 1H), 7.55 (d, $J = 8$ Hz, 1H), 7.35 (t, $J = 8$ Hz, 1H), 7.32 (s, 1H), 7.16 (d, $J = 8$ Hz, 1H), 7.10 (t, $J = 8$ Hz, 1H), 7.03 (d, $J = 8$ Hz, 1H), 6.97 (d, $J = 8$ Hz, 1H), 3.84 (s, 3H), 3.82 (s, 3H); ^{13}C NMR: 166.7, 163.7, 157.1, 151.4, 149.6, 149.2, 146.1, 142.0, 133.4, 131.3, 127.6, 123.0, 122.5, 120.5, 120.1, 118.4, 112.1, 111.6, 109.0, 56.1; anal. calcd. for $\text{C}_{21}\text{H}_{18}\text{N}_6\text{O}_4\text{S}$: C, 55.99; H,

4.03; N, 18.66; S, 7.12. Found: C, 56.14; H, 4.08; N, 18.79; S, 7.23.

2-[2-((*Z*)-2-Oxoindolin-3-ylidene)hydrazineyl]-*N'*-((*E*)-1-phenylethylidene)thiazole-4-carbohydrazide **4j**. Yellow solid; yield 0.19 g (70%); mp 280–283 °C; FT-IR: 3392, 3329, 3121, 1683, 1651, 1617, 1558, 1489, 1466, 1166; ^1H NMR: 13.31 (s, 1H), 11.28 (s, 1H), 10.51 (s, 1H), 7.99 (s, 1H), 7.87, (m, 2H), 7.57 (d, $J = 8$ Hz, 1H), 7.46 (m, 3H), 7.37 (t, $J = 8$ Hz, 1H), 7.12 (t, $J = 6$ Hz, 1H), 6.98 (d, $J = 8$ Hz, 1H), 2.39 (s, 3H); ^{13}C NMR: 166.9, 163.6, 142.0, 138.3, 131.4, 130.1, 128.9, 127.0, 123.0, 121.9, 120.6, 120.1, 118.5, 111.6, 14.3; anal. calcd. for $\text{C}_{20}\text{H}_{16}\text{N}_6\text{O}_2\text{S}$: C, 59.39; H, 3.99; N, 20.78; S, 7.93. Found: C, 59.60; H, 4.14; N, 21.04; S, 7.69.

N'-((*E*)-Furan-2-ylmethylene)-2-[2-((*Z*)-2-oxoindolin-3-ylidene)hydrazineyl]thiazole-4-carbohydrazide **4k**. Yellow solid; yield 0.18 g (72%); mp 295–296 °C; FT-IR: 3440, 3287, 3227, 3129, 1686, 1661, 1619, 1558, 1496, 1466, 1174; ^1H NMR: 13.36 (s, 1H), 11.88 (s, 1H), 11.28 (s, 1H), 8.45 (s, 1H), 7.96 (s, 1H), 7.86 (m, 1H), 7.57 (d, $J = 4$ Hz, 1H), 7.37 (t, $J = 8$ Hz, 1H), 7.11 (t, $J = 8$ Hz, 1H), 6.98 (d, $J = 8$ Hz, 1H), 6.92 (d, $J = 4$ Hz, 1H), 6.65 (m, 1H); ^{13}C NMR: 166.7, 163.7, 157.2, 150.0, 145.8, 145.7, 142.0, 138.6, 133.5, 131.3, 123.0, 120.6, 120.0, 118.8, 113.9, 112.7, 111.6; anal. calcd. for $\text{C}_{17}\text{H}_{12}\text{N}_6\text{O}_3\text{S}$: C, 53.68; H, 3.18; N, 22.09; S, 8.43. Found: C, 53.75; H, 3.42; N, 22.37; S, 8.60.

2-[2-((*Z*)-2-Oxoindolin-3-ylidene)hydrazineyl]-*N'*-((1*E*,2*E*)-3-phenylallylidene)thiazole-4-carbohydrazide **4l**. Yellow solid; yield 0.25 g (89%); mp 299–300 °C; FT-IR: 3440, 3302, 3156, 1696, 1680, 1655, 1624, 1560, 1497, 1467, 1159; ^1H NMR: 13.36 (s, 1H), 11.79 (s, 1H), 11.28 (s, 1H), 8.36 (d, $J = 8$ Hz, 1H), 7.95 (s, 1H), 7.64 (d, $J = 8$ Hz, 2H), 7.57 (d, $J = 8$ Hz, 1H), 7.42–7.37 (m, 3H), 7.35–7.32 (m, 1H), 7.11 (t, $J = 8$ Hz, 1H), 7.06–6.97 (m, 3H); ^{13}C NMR: 166.7, 163.7, 157.2, 150.9, 145.9, 142.0, 139.5, 136.4, 133.5, 131.3, 129.3, 127.6, 126.3, 123.0, 120.6, 120.0, 118.7, 111.6; ESI-MS m/z : 416.25 [M^+]; anal. calcd. for $\text{C}_{21}\text{H}_{16}\text{N}_6\text{O}_2\text{S}$: C, 60.56; H, 3.87; N, 20.18; S, 7.70. Found: C, 60.82; H, 3.62; N, 20.43; S, 7.78.

N'-((*Z*)-2-Oxoindolin-3-ylidene)-2-[2-((*Z*)-2-oxoindolin-3-ylidene)hydrazineyl]thiazole-4-carbohydrazide **4m**. Yellow solid; yield 0.22 g (76%); mp >300 °C; FT-IR: 3336, 3216, 3110, 1678, 1619, 1560, 1491, 1468, 1138; ^1H NMR: 14.07 (s, 1H), 13.36 (s, 1H), 11.33 (s, 1H), 11.26 (s, 1H), 8.16 (s, 1H), 7.63–7.58 (m, 2H), 7.43–7.37 (m, 2H), 7.14–7.11 (m, 2H), 7.00–6.97 (m, 2H); ^{13}C NMR: 167.2, 163.7, 163.0, 157.6, 144.9, 143.2, 142.2, 138.7, 133.9, 132.3, 131.5, 123.1, 123.0, 121.5, 120.7, 120.0, 111.6; anal. calcd. for $\text{C}_{20}\text{H}_{13}\text{N}_7\text{O}_3\text{S}$: C, 55.68; H, 3.04; N, 22.73; S, 7.43. Found: C, 55.75; H, 3.16; N, 22.98; S, 7.50.

N'-((*Z/E*)-5-Methoxy-2-oxoindolin-3-ylidene)-2-[2-((*Z*)-2-oxoindolin-3-ylidene)hydrazineyl]thiazole-4-carbohydrazide **4n**. Yellow solid; yield 0.26 g (84%); mp 297–299 °C; FT-IR: 3364, 3289, 3119, 1730, 1689, 1619, 1553, 1498, 1467, 1165; ^1H NMR: 14.08 (s, 1H), 13.35 (s, 1H), 11.32 (s, 1H), 11.06 (s, 1H), 8.15 (s, 1H), 7.56 (d, $J = 8$ Hz, 1H), 7.39–7.35 (m, 1H), 7.14–7.05 (m, 2H), 6.98 (d, $J = 8$ Hz, 1H), 6.95 (s, 1H), 6.88 (d, $J = 8$ Hz, 1H), 3.79 (s, 3H); ^{13}C NMR: 167.1, 163.7, 163.1, 157.6, 155.8, 155.0, 144.7, 142.1, 139.1, 138.2, 136.8, 134.0, 133.8,

131.5, 123.0, 121.1, 120.8, 120.7, 120.0, 118.8, 116.1, 112.5, 111.7, 106.2, 56.1; anal. calcd. for $C_{21}H_{15}N_7O_4S$: C, 54.66; H, 3.28; N, 21.25; S, 6.95. Found: C, 54.79; H, 3.40; N, 21.49; S, 6.81.

N'-((Z/E)-5-Fluoro-2-oxoindolin-3-ylidene)-2-[2-((Z)-2-oxoindolin-3-ylidene)hydrazineyl]thiazole-4-carbohydrazide 4o. Yellow solid; yield 0.24 g (80%); mp >300 °C; FT-IR: 3180, 3128, 1746, 1687, 1622, 1561, 1480, 1468, 1158; 1H NMR: 13.48 (s, 1H), 11.51 (s, 1H), 11.30 (s, 1H), 10.92 (s, 1H), 8.20 (s, 1H), 7.59–7.57 (m, 1H), 7.44–7.35 (m, 3H), 7.11 (t, J = 8 Hz, 1H), 6.99–6.95 (m, 2H); ^{13}C NMR: 166.7, 166.6, 164.5, 163.5, 163.2, 162.6, 159.5, 158.4, 157.7, 157.1, 156.4, 156.1, 146.1, 144.2, 141.9, 141.7, 140.3, 138.9, 137.9, 133.4, 133.3, 131.0, 122.5, 121.1, 120.9, 120.5, 120.2, 119.5, 119.2, 115.8, 113.0, 112.7, 112.2, 112.0, 111.2, 108.2, 108.0; anal. calcd. for $C_{20}H_{12}FN_7O_3S$: C, 53.45; H, 2.69; N, 21.82; S, 7.13. Found: C, 53.72; H, 2.78; N, 21.73; S, 7.15.

3.1.5. General procedure for synthesis of compounds 5a–c.

A mixture of acid anhydride (0.66 mmol) was added to a solution of **3** (0.2 g, 0.66 mmol) in toluene (15 mL). The mixture was refluxed for the specified time (18–24 h). After cooling to room temperature, the precipitate was filtered and dried. The crude precipitate was purified by column chromatography on silica gel with dichloromethane/methanol to afford **5a–c** in yield of 80–86%.

(Z)-N-(2,5-Dioxopyrrolidin-1-yl)-2-[2-(2-oxoindolin-3-ylidene)hydrazineyl]thiazole-4-carboxamide 5a. Yellow solid; yield 0.2 g (80%); mp 281–283 °C; FT-IR: 3509, 3188, 3116, 1720, 1690, 1618, 1556, 1466, 1161; 1H NMR: 11.28 (s, 1H), 10.12 (s, 1H), 9.95 (s, 1H), 7.87 (s, 1H), 7.56 (d, J = 8 Hz, 1H), 7.37 (t, J = 8 Hz, 1H), 7.11 (t, J = 8 Hz, 1H), 6.98 (d, J = 8 Hz, 1H), 2.50–2.43 (m, 4H); ^{13}C NMR: 174.0, 170.6, 166.7, 163.7, 159.8, 145.5, 142.0, 133.4, 131.3, 123.0, 120.5, 120.1, 118.2, 111.6, 29.3, 28.6; anal. calcd. for $C_{16}H_{12}N_6O_4S$: C, 50.00; H, 3.15; N, 21.86; S, 8.34. Found: C, 50.21; H, 3.34; N, 22.04; S, 8.39.

(Z)-N-(1,3-Dioxoisindolin-2-yl)-2-[2-(2-oxoindolin-3-ylidene)hydrazineyl]thiazole-4-carboxamide 5b. Yellow solid; yield 0.25 g (86%); mp 296–298 °C; FT-IR: 3339, 3204, 3105, 1742, 1703, 1680, 1622, 1543, 1466, 1185; 1H NMR: 11.58 (s, 1H), 11.24 (s, 1H), 11.13 (s, 1H), 8.08 (s, 1H), 8.05 (s, 1H), 7.98 (s, 1H), 7.95 (s, 1H), 7.87 (s, 1H), 7.52 (d, J = 8 Hz, 1H), 7.34 (t, J = 6 Hz, 1H), 7.09 (t, J = 6 Hz, 1H), 6.96 (d, J = 8 Hz, 1H); ^{13}C NMR: 167.2, 165.5, 163.7, 159.9, 155.2, 143.9, 142.0, 135.8, 133.6, 133.0, 131.3, 129.8, 127.6, 125.6, 124.3, 123.0, 120.6, 120.2, 119.9, 111.6; anal. calcd. for $C_{20}H_{12}N_6O_4S$: C, 55.55; H, 2.80; N, 19.44; S, 7.42. Found: C, 55.73; H, 3.07; N, 19.70; S, 7.53.

(Z)-N-(7,9-Dioxo-8-azaspiro[4.5]decan-8-yl)-2-[2-(2-oxoindolin-3-ylidene)hydrazineyl]thiazole-4-carboxamide 5c. Yellow solid; yield 0.25 g (83%); mp 287–290 °C; FT-IR: 3400, 3329, 3266, 3185, 3061, 2955, 1683, 1618, 1559, 1491, 1466, 1166; 1H NMR: 13.39 (s, 1H), 11.27 (s, 1H), 10.58 (s, 1H), 7.90 (s, 1H), 7.57 (d, J = 8 Hz, 1H), 7.37 (t, J = 8 Hz, 1H), 7.11 (t, J = 8 Hz, 1H), 6.98 (d, J = 8 Hz, 1H), 2.77 (d, J = 8 Hz, 4H), 1.66–1.51 (m, 8H); ^{13}C NMR: 170.1, 166.9, 163.7, 159.2, 144.6, 142.0, 133.5, 131.4, 123.0, 120.6, 120.0, 119.2, 111.6, 43.9, 37.2, 37.0,

23.9; anal. calcd. for $C_{21}H_{20}N_6O_4S$: C, 55.74; H, 4.46; N, 18.57; S, 7.09. Found: C, 55.97; H, 4.42; N, 18.73; S, 7.23.

3.1.6. General procedure for synthesis of compounds 6a–d.

A mixture of substituted isothiocyanate (1.32 mmol) was added to a solution of **3** (0.4 g, 1.32 mmol) in absolute ethanol (15 mL). The reaction mixture was refluxed for the specified time (18–24 h). After cooling to room temperature, the precipitate was filtered and dried. The crude precipitate was recrystallized from methanol to yield **6a–d** (68–81%).

(Z)-N-Ethyl-2-[2-(2-oxoindolin-3-ylidene)hydrazineyl]thiazole-4-carbonyl]hydrazine-1-carbothioamide 6a. Yellow solid; yield 0.42 g (81%); mp 270–272 °C; FT-IR: 3328, 3197, 3139, 1688, 1662, 1622, 1562, 1492, 1467, 1159; 1H NMR: 13.26 (s, 1H), 11.27 (s, 1H), 10.18 (s, 1H), 9.24 (s, 1H), 7.96 (s, 1H), 7.90 (s, 1H), 7.55 (d, J = 8 Hz, 1H), 7.36 (t, J = 8 Hz, 1H), 7.10 (t, J = 8 Hz, 1H), 6.97 (d, J = 8 Hz, 1H), 3.44 (q, J = 6.7 Hz, 2H), 1.05 (t, J = 8 Hz, 3H); ^{13}C NMR: 181.0, 165.9, 163.2, 159.9, 145.1, 141.5, 132.9, 130.8, 122.5, 120.1, 119.5, 118.0, 111.2, 38.5, 14.5; anal. calcd. for $C_{15}H_{15}N_7O_2S_2$: C, 46.26; H, 3.88; N, 25.18; S, 16.47. Found: C, 46.39; H, 4.03; N, 25.42; S, 16.59.

(Z)-2-[2-(2-Oxoindolin-3-ylidene)hydrazineyl]thiazole-4-carbonyl]-N-phenylhydrazine-1-carbothioamide 6b. Yellow solid; yield 0.47 g (81%); mp 213–215 °C FT-IR: 3315, 3202, 3120, 1675, 1618, 1557, 1498, 1465, 1170; 1H NMR: 11.30 (s, 1H), 10.44 (s, 1H), 9.74 (s, 3H), 7.95 (s, 1H), 7.58–7.55 (m, 2H), 7.47 (m, 1H), 7.39–7.31 (m, 3H), 7.18–7.09 (m, 2H), 6.98 (d, J = 8 Hz, 1H); ^{13}C NMR: 180.8, 166.1, 165.9, 163.2, 159.7, 145.5, 145.1, 141.5, 139.3, 132.9, 132.7, 130.8, 128.1, 128.0, 124.7, 122.5, 120.1, 119.5, 118.0, 116.2, 111.1; anal. calcd. for $C_{19}H_{15}N_7O_2S_2$: C, 52.16; H, 3.46; N, 22.41; S, 14.66. Found: C, 52.42; H, 3.68; N, 22.69; S, 14.71.

(Z)-2-[2-(2-Oxoindolin-3-ylidene)hydrazineyl]thiazole-4-carbonyl]-N-(p-tolyl)hydrazine-1-carbothioamide 6c. Yellow solid; yield 0.47 g (78%); mp 291–293 °C; 1H NMR: 13.36 (s, 1H), 11.28 (s, 1H), 10.37 (s, 1H), 9.66 (s, 2H), 7.93 (s, 1H), 7.57 (d, J = 8 Hz, 1H), 7.37 (t, J = 8 Hz, 1H), 7.33 (m, 2H), 7.16–7.09 (m, 3H), 6.98 (d, J = 8 Hz, 1H), 2.28 (s, 3H); ^{13}C NMR: 181.3, 166.4, 163.7, 145.6, 142.0, 137.2, 134.5, 133.3, 131.3, 128.9, 126.0, 123.0, 120.5, 120.0, 118.4, 111.6, 21.0; ESI-MS m/z : 451.17 [M^+]; anal. calcd. for $C_{20}H_{17}N_7O_2S_2$: C, 53.20; H, 3.79; N, 21.71; S, 14.20. Found: C, 53.41; H, 3.95; N, 21.98; S, 14.09.

(Z/E)-N-(4-Chlorophenyl)-2-[2-(2-oxoindolin-3-ylidene)hydrazineyl]thiazole-4-carbonyl]hydrazine-1-carbothioamide 6d. Yellow solid; yield 0.42 g (68%); mp >300 °C; FT-IR: 3409, 3324, 3121, 1683, 1656, 1618, 1558, 1493, 1466, 1166; 1H NMR: 11.25 (s, 1H), 9.61 (s, 1H), 8.96 (s, 1H), 8.28 (s, 1H), 7.76 (s, 1H), 7.56–7.48 (m, 3H), 7.36 (t, J = 8 Hz, 1H), 7.31 (d, J = 8 Hz, 2H), 7.10 (t, J = 8 Hz, 1H), 6.98 (d, J = 8 Hz, 1H); ^{13}C NMR: 166.5, 163.7, 160.1, 156.4, 146.1, 145.6, 141.9, 139.2, 133.2, 131.2, 128.9, 125.9, 123.0, 120.5, 120.1, 118.3, 116.5, 111.6; anal. calcd. for $C_{19}H_{14}ClN_7O_2S_2$: C, 48.35; H, 2.99; N, 20.78; S, 13.59. Found: C, 48.62; H, 3.15; N, 20.65; S, 13.63.

3.1.7. General procedure for synthesis of compounds 7a–d.

To a solution of **6a–d** (0.5 mmol) in DMSO (10 mL),

potassium bisulfate (4 mmol) was added. The mixture was heated at 50 °C for the specified time (36–48 h). After the completion of the reaction, the mixture was diluted with 30 mL of water. The precipitate was filtered and dried. The crude precipitate was purified by column chromatography on silica gel with dichloromethane/methanol to afford **7a–d** in yield (62–67%).

(*Z*)-3-(2-[4-(5-(Ethylamino)-1,3,4-oxadiazol-2-yl)thiazol-2-yl]hydrazineylidene)indolin-2-one **7a**. Yellow solid; yield 0.12 g (67%); mp 279–281 °C; ¹H NMR: 13.35 (s, 1H), 11.29 (s, 1H), 7.81 (t, *J* = 4 Hz, 1H), 7.70 (s, 1H), 7.56 (d, *J* = 8 Hz, 1H), 7.37 (t, *J* = 8 Hz, 1H), 7.11 (t, *J* = 8 Hz, 1H), 6.98 (d, *J* = 8 Hz, 1H), 3.31–3.24 (m, 2H), 1.19 (t, *J* = 6 Hz, 3H); ¹³C NMR: 167.8, 163.6, 154.3, 142.1, 137.2, 133.4, 131.3, 122.9, 120.6, 120.0, 113.5, 111.6, 37.9, 15.0; anal. calcd. for C₁₅H₁₃N₇O₂S: C, 50.70; H, 3.69; N, 27.59; S, 9.02. Found: C, 50.94; H, 3.80; N, 27.78; S, 9.23.

(*Z*)-3-(2-[4-(5-(Phenylamino)-1,3,4-oxadiazol-2-yl)thiazol-2-yl]hydrazineylidene)indolin-2-one **7b**. Yellow solid; yield 0.13 g (65%); mp 245–248 °C; FT-IR: 3139, 1695, 1620, 1601, 1552, 1499, 1466, 1155; ¹H NMR: 13.37 (s, 1H), 11.26 (s, 1H), 10.71 (s, 1H), 7.81 (s, 1H), 7.61 (d, *J* = 8 Hz, 2H), 7.56 (d, *J* = 8 Hz, 1H), 7.37 (m, 3H), 7.10 (t, *J* = 8 Hz, 1H), 7.02 (t, *J* = 8 Hz, 1H), 6.97 (d, *J* = 8 Hz, 1H); ¹³C NMR: 168.0, 163.6, 160.0, 154.5, 142.1, 139.0, 136.7, 133.6, 131.4, 129.6, 123.0, 122.5, 120.6, 120.0, 117.6, 114.7, 111.6; anal. calcd. for C₁₉H₁₃N₇O₂S: C, 56.57; H, 3.25; N, 24.30; S, 7.95. Found: C, 56.83; H, 3.44; N, 24.69; S, 7.84.

(*Z*)-3-(2-[4-(5-(*p*-Tolylamino)-1,3,4-oxadiazol-2-yl)thiazol-2-yl]hydrazineylidene)indolin-2-one **7c**. Yellow solid; yield 0.13 g (62%); mp 256–258 °C; ¹H NMR: 13.37 (s, 1H), 11.27 (s, 1H), 10.60 (s, 1H), 7.57 (d, *J* = 8 Hz, 1H), 7.50 (d, *J* = 8 Hz, 2H), 7.37 (t, *J* = 8 Hz, 1H), 7.27 (s, 1H), 7.18 (d, *J* = 8 Hz, 2H), 7.11 (t, *J* = 8 Hz, 1H), 6.99 (d, *J* = 8 Hz, 1H), 2.28 (s, 3H); ¹³C NMR: 167.9, 163.6, 160.1, 154.4, 142.1, 136.8, 136.5, 133.6, 131.3, 130.0, 123.0, 120.6, 120.1, 117.6, 114.5, 111.6, 20.8; anal. calcd. for C₂₀H₁₅N₇O₂S: C, 57.54; H, 3.62; N, 23.49; S, 7.68. Found: C, 57.71; H, 3.69; N, 23.72; S, 7.75.

(*Z*)-3-(2-[4-(5-(4-Chlorophenyl)amino)-1,3,4-oxadiazol-2-yl]thiazol-2-yl]hydrazineylidene)indolin-2-one **7d**. Yellow solid; yield 0.14 g (64%); mp 288–290 °C; FT-IR: 3431, 1687, 1605, 1552, 1494, 1469, 1155; ¹H NMR: 13.37 (s, 1H), 11.29 (s, 1H), 8.98 (s, 1H), 8.10 (s, 1H), 7.57–7.52 (m, 3H), 7.38 (t, *J* = 6 Hz, 1H), 7.32 (d, *J* = 12 Hz, 2H), 7.12 (t, *J* = 8 Hz, 1H), 6.99 (d, *J* = 8 Hz, 1H); ¹³C NMR: 163.7, 162.8, 156.4, 145.6, 142.0, 139.2, 133.4, 128.9, 125.9, 123.0, 120.6, 120.1, 118.3, 111.6; anal. calcd. for C₁₉H₁₂ClN₇O₂S: C, 52.12; H, 2.76; N, 22.39; S, 7.32. Found: C, 52.40; H, 2.94; N, 22.57; S, 7.40.

3.1.8. Synthesis of (*Z/E*)-2-(2-[2-(2-Oxoindolin-3-ylidene)hydrazineyl]thiazole-4-carbonyl)hydrazine-1-carbothioamide

8. To a solution of **3** (0.5 g, 1.65 mmol) in DMF (20 mL), ammonium thiocyanate (0.13 g, 1.65 mmol), and 0.3 mL of hydrochloric acid were added. The reaction mixture was heated at 100 °C for 24 h. The mixture was diluted with 40 mL of water. The precipitate was filtered, dried, and recrystallized from ethanol.

Yellow solid; yield 0.5 g (83%); mp 297–298 °C; FT-IR: 3380, 3159, 3119, 1715, 1694, 1619, 1554, 1464, 1150; ¹H NMR: 11.25 (s, 1H), 10.20 (s, 1H), 10.01 (s, 1H), 8.07 (s, 1H), 7.88 (s, 1H), 7.54 (d, *J* = 8 Hz, 1H), 7.35 (t, *J* = 8 Hz, 1H), 7.09 (t, *J* = 8 Hz, 1H), 6.96 (d, *J* = 8 Hz, 1H); ¹³C NMR: 166.9, 166.4, 166.2, 163.2, 161.0, 159.6, 159.2, 144.7, 144.4, 141.5, 133.0, 132.9, 130.9, 130.8, 122.5, 120.1, 119.6, 119.5, 118.5, 118.0, 111.1; anal. calcd. for C₁₃H₁₁N₇O₂S₂: C, 43.20; H, 3.07; N, 27.13; S, 17.74. Found: C, 43.47; H, 3.20; N, 27.41; S, 17.85.

3.1.9. Synthesis of (*Z*)-*N'*-(4-(4-bromophenyl)thiazol-2-yl)-2-[2-(2-oxoindolin-3-ylidene)hydrazineyl]thiazole-4-carbohydrazide **10**

To a mixture of compound **8** (0.2 g, 0.55 mmol) in absolute ethanol (15 mL), 4-bromophenacyl bromide **9a** (0.55 mmol) was added. The reaction mixture was refluxed for 10 h until the reaction ended. After cooling to room temperature, the precipitate was filtered and dried. The crude precipitate was triturated several times with diethyl ether and filtered.

Brown solid; yield 0.24 g (80%); mp 240–242 °C; FT-IR: 3392, 3265, 3106, 1727, 1701, 1620, 1552, 1465, 1160. ¹H NMR: 13.32 (s, 1H), 11.26 (s, 1H), 8.18 (s, 1H), 7.96 (d, *J* = 8 Hz, 2H), 7.82 (d, *J* = 8 Hz, 2H), 7.75 (s, 1H), 7.57 (d, *J* = 8 Hz, 1H), 7.37 (t, *J* = 8 Hz, 1H), 7.11 (t, *J* = 8 Hz, 1H), 6.98 (d, *J* = 8 Hz, 1H), 5.71 (s, 1H); ¹³C NMR: 166.8, 163.6, 163.4, 160.3, 145.4, 142.2, 142.0, 135.3, 133.4, 132.0, 131.3, 129.5, 129.1, 123.9, 122.9, 120.5, 119.9, 119.4, 111.6; anal. calcd. for C₂₁H₁₄BrN₇O₂S₂: C, 46.67; H, 2.61; N, 18.14; S, 11.87. Found: C, 46.96; H, 2.85; N, 18.40; S, 11.98.

3.1.10. Synthesis of (*Z/E*)-3-(2-[4-(5-Thioxo-4,5-dihydro-1,3,4-oxadiazol-2-yl)thiazol-2-yl]hydrazineylidene)indolin-2-one **11**

To a mixture of **3** (1 g, 3.3 mmol) in 20 mL of absolute ethanol and potassium hydroxide (0.2 g, 3.6 mmol), carbon disulfide (1.6 mL, 26.4 mmol) was added. The mixture was refluxed for 24 h. After the completion of the reaction, the mixture was cooled to room temperature. The solvent was completely evaporated, the residue dissolved in water and filtered. The filtrate was acidified with 10% HCl. The precipitate was filtered, dried, and recrystallized from ethanol.

Yellow solid; yield 0.85 g (77%); mp 295–298 °C; FT-IR: 3115, 1714, 1686, 1622, 1557, 1466, 1159; ¹H NMR: 14.61 (s, 1H), 13.34 (s, 1H), 11.26 (s, 1H), 8.02 (s, 1H), 7.56 (s, 1H), 7.35 (s, 1H), 7.09–6.89 (m, 2H); ¹³C NMR: 177.6, 168.2, 164.9, 163.5, 156.9, 143.6, 142.2, 135.4, 133.9, 132.4, 131.5, 123.0, 122.1, 120.7, 120.0, 117.7, 111.6; anal. calcd. for C₁₃H₈N₆O₂S₂: C, 45.34; H, 2.34; N, 24.40; S, 18.62. Found: C, 45.62; H, 2.39; N, 24.63; S, 18.84.

3.1.11. General procedure for synthesis of compounds **12a–e**

To a mixture of **11** (0.2 g, 0.58 mmol) in 10 mL of acetonitrile and potassium carbonate (0.08 g, 0.58 mmol), substituted phenacyl bromide **9b**, **c** or substituted benzyl chloride (0.58 mmol) were added. The reaction mixture was stirred for (6–8 h) at room temperature. The precipitate was filtered, washed with water and dried. The crude product was triturated several times with diethyl ether and filtered to yield **12a–e** (67–89%).

(*Z*)-3-(2-[4-(5-((2-Oxo-2-phenylethyl)thio)-1,3,4-oxadiazol-2-yl)thiazol-2-yl]hydrazineylidene)indolin-2-one **12a**. Yellow solid; yield 0.24 g (89%); mp 292–295 °C; FT-IR: 3420, 3281, 3107, 2915, 1708, 1684, 1553, 1466, 1161; ¹H NMR: 13.37 (s, 1H), 11.28 (s, 1H), 8.09 (d, *J* = 8 Hz, 2H), 8.05 (s, 1H), 7.74 (m, 1H), 7.62 (d, *J* = 8 Hz, 2H), 7.58 (d, *J* = 8 Hz, 1H), 7.38 (t, *J* = 8 Hz, 1H), 7.12, (t, *J* = 8 Hz, 1H), 6.99 (d, *J* = 8 Hz, 1H), 5.21 (s, 2H); ¹³C NMR: 193.0, 168.2, 163.5, 161.5, 142.2, 135.9, 135.5, 134.5, 133.8, 131.4, 129.4, 129.0, 123.0, 120.6, 120.0, 117.2, 111.6, 41.2; anal. calcd. for C₂₁H₁₄N₆O₃S₂: C, 54.53; H, 3.05; N, 18.17; S, 13.87. Found: C, 54.67; H, 3.21; N, 18.45; S, 13.74.

(*Z*)-3-(2-[4-(5-((2-Oxo-2-(*p*-tolyl)ethyl)thio)-1,3,4-oxadiazol-2-yl)thiazol-2-yl]hydrazineylidene)indolin-2-one **12b**. Yellow solid; yield 0.23 g (82%); mp 277–279 °C; FT-IR: 3224, 3111, 2919, 1699, 1677, 1552, 1469, 1158; ¹H NMR: 13.38 (s, 1H), 11.31 (s, 1H), 8.05 (s, 1H), 7.99 (d, *J* = 8 Hz, 2H), 7.57 (d, *J* = 8 Hz, 1H), 7.42 (d, *J* = 8 Hz, 2H), 7.38 (t, *J* = 8 Hz, 1H), 7.12 (t, *J* = 6 Hz, 1H), 6.99 (d, *J* = 8 Hz, 1H), 5.18 (s, 2H), 2.43 (s, 3H); ¹³C NMR: 192.5, 168.2, 163.6, 163.5, 142.2, 133.8, 133.0, 129.9, 129.1, 123.0, 120.7, 120.0, 117.2, 114.4, 113.4, 113.2, 111.6, 41.2, 21.7; anal. calcd. for C₂₂H₁₆N₆O₃S₂: C, 55.45; H, 3.38; N, 17.64; S, 13.46. Found: C, 55.71; H, 3.45; N, 17.89; S, 13.35.

(*Z*)-3-(2-[4-(5-(Benzylthio)-1,3,4-oxadiazol-2-yl)thiazol-2-yl]hydrazineylidene)indolin-2-one **12c**. Yellow solid; yield 0.19 g (76%); mp 277–279 °C; FT-IR: 3316, 3105, 2927, 1707, 1619, 1568, 1484, 1467, 1163; ¹H NMR: 13.36 (s, 1H), 11.27 (s, 1H), 8.04 (s, 1H), 7.55 (d, *J* = 8 Hz, 1H), 7.49 (d, *J* = 8 Hz, 2H), 7.38–7.34 (m, 3H), 7.30 (t, *J* = 8 Hz, 1H), 7.10 (t, *J* = 8 Hz, 1H), 6.97 (d, *J* = 8 Hz, 1H), 4.59 (s, 2H); ¹³C NMR: 168.2, 163.5, 161.6, 142.2, 136.9, 136.0, 133.8, 131.4, 129.6, 129.5, 129.1, 128.3, 123.0, 120.6, 120.0, 117.2, 111.6, 36.5; anal. calcd. for C₂₀H₁₄N₆O₂S₂: C, 55.29; H, 3.25; N, 19.34; S, 14.76. Found: C, 55.47; H, 3.53; N, 19.57; S, 14.62.

(*Z*)-3-(2-[4-(5-((4-Chlorobenzyl)thio)-1,3,4-oxadiazol-2-yl)thiazol-2-yl]hydrazineylidene)indolin-2-one **12d**. Yellow solid; yield 0.21 g (78%); mp 214–216 °C; FT-IR: 3278, 3140, 3100, 2930, 1705, 1619, 1565, 1482, 1465, 1163; ¹H NMR: 8.18 (s, 1H), 7.58 (m, 1H), 7.51 (d, *J* = 8 Hz, 2H), 7.42 (d, *J* = 8 Hz, 2H), 7.01 (t, *J* = 8 Hz, 1H), 6.87 (t, *J* = 8 Hz, 1H), 6.75 (d, *J* = 8 Hz, 1H), 4.56 (s, 2H); ¹³C NMR: 167.0, 163.0, 162.2, 139.3, 136.3, 136.1, 132.9, 131.4, 129.0, 128.8, 126.2, 123.7, 120.8, 120.2, 116.4, 114.8, 108.8, 35.6; anal. calcd. for C₂₀H₁₃ClN₆O₂S₂: C, 51.22; H, 2.79; N, 17.92; S, 13.68. Found: C, 51.43; H, 2.95; N, 18.16; S, 13.75.

(*Z*)-3-(2-[4-(5-((4-Methoxybenzyl)thio)-1,3,4-oxadiazol-2-yl)thiazol-2-yl]hydrazineylidene)indolin-2-one **12e**. Yellow solid; yield 0.18 g (67%); mp 242–245 °C; FT-IR: 3428, 3166, 3101, 2966, 1719, 1611, 1549, 1474, 1464, 1157; ¹H NMR: 13.36 (s, 1H), 11.28 (s, 1H), 8.05 (s, 1H), 7.56 (m, 1H), 7.42–7.40 (m, 2H), 7.37 (m, 1H), 7.10 (m, 1H), 6.98 (m, 1H), 6.92–6.87 (m, 1H), 4.54 (s, 2H), 3.74 (s, 3H); ¹³C NMR: 168.2, 163.5, 159.4, 142.2, 136.0, 133.8, 131.5, 130.9, 128.5, 123.0, 121.1, 120.7, 120.0, 117.2, 114.6, 114.5, 111.6, 55.6, 36.2; anal. calcd. for C₂₁H₁₆N₆O₃S₂: C, 54.30; H, 3.47; N, 18.09; S, 13.81. Found: C, 54.53; H, 3.62; N, 18.24; S, 13.95.

3.2. Biological investigation

3.2.1. *In vitro* antiproliferative screening against NCI cancer cell lines. The methodology of the NCI procedures for anticancer screening for primary single-dose and five-dose assays was illustrated on the website (https://dtp.cancer.gov/discovery_development/nci-60/methodology.htm). The NCI *in vitro* screening is a two-stage process, beginning with the evaluation of the synthesized compounds against the full NCI-60 cell line panel derived from nine different human cancers at a single high dose of 10 μM according to NCI standard procedure. The output from the single-dose screening is reported as a mean graph, as shown in the ESI.† Secondly, only the compounds **4b**, **4c**, **4d**, **4l**, and **6c**, which had significant growth inhibition across multiple cell lines, were selected for the full five-dose assay. The result from the five-dose screening was reported as growth inhibition curves and three response parameters (GI₅₀, TGI, and LC₅₀) for each cell line, as presented in the ESI.†

3.2.2. *In vitro* cytotoxicity screening against hepatocellular carcinoma (HepG2) and normal liver cell line (THLE-2). The cytotoxicity of the target compounds **4b**, **4c**, **4d**, **4l**, and **6c** was inspected using the 3-(4,5-dimethylthiazol-2-yl)-2,5-diphenyltetrazolium bromide (MTT) assay against hepatic cancer cell line (HepG2) and non-tumorigenic human liver epithelial cell line (THLE-2), as reported in the ESI.†

3.2.3. *In vitro* VEGFR-2 kinase inhibitory assay. The VEGFR-2 kinase inhibition assay was performed for the compounds **4b**, **4c**, **4d**, **4l**, and **6c** through a reported methodology using the VEGFR2(KDR) Assay Kit (Enzyme-Linked Immunosorbent Assay), as described in the ESI.†

3.2.4. Cell cycle analysis. The compound **4c** was further assessed through cell cycle analysis in HepG2 cells to determine the cell cycle distribution using propidium iodide (PI) staining and flow cytometry analysis, as shown in the ESI.†

3.2.5. Apoptosis analysis. The effects of compound **4c** on the induction of apoptosis and necrosis in the hepatic cancer cell line (HepG2) were investigated using the annexin V-FITC/PI dual staining by flow cytometric analysis, as presented in the ESI.†

3.2.6. Caspases-3 and -9 expression assay. The level of the apoptotic markers caspase-3 and -9 in the hepatic HepG2 cells treated with 5.67 μM of compound **4c** was assessed using the real-time quantitative PCR of RNA template analysis, as determined in the ESI.†

3.2.7. *In vitro* wound healing assay. The effect of compound **4c** on the HepG2 cell proliferation and migration was fulfilled as reported in the ESI.†

3.3. Molecular modeling studies

3.3.1. Docking study. The molecular docking study was achieved using Molecular Operating Environment software version MOE 2020.09. The docking protocol is reported in the ESI.†

3.3.2. *In silico* prediction of physicochemical and pharmacokinetic properties. The physicochemical parameters

of drug-likeness and the pharmacokinetic properties of the most potent synthesized compounds **4b**, **4c**, **4d**, **4l**, and **6c** in comparison with sunitinib were calculated using the free SwissADME web tool (<http://www.swissadme.ch/accessed> 26 July 2024) available from the Swiss Institute of Bioinformatics for the calculations.

3.3.3. DFT (quantum chemistry calculations and the electron density map). Gaussian 09 program was utilized for quantum chemistry calculations and the electron density map of the most active compounds **4c**, as outlined thoroughly in the ESI.†

4. Conclusion

In this study, new 2-oxoindolin-3-ylidene thiazole derivatives were designed and synthesized based on the reported pharmacophoric features of VEGFR-2 inhibitors. The target compounds were tested for their antiproliferative activity against NCI cell line panel as well as *in vitro* VEGFR-2 inhibitory activities. Compounds **4b**, **4c**, **4d**, **4l**, and **6c** exhibited potent cytotoxicity with GI₅₀ values ranging from 1.67 to 30.2 μM. Additionally, Compounds **4b**, **4c**, **4d**, **4l**, and **6c** displayed promising VEGFR-2 inhibitory activities with IC₅₀ of 0.113, 0.047, 1.549, 0.995, and 0.089 μM, respectively, compared to sunitinib with IC₅₀ of 0.167 μM. Furthermore, the target compounds exhibited lower cytotoxicity against normal THLE-2 cells compared to HepG2 cells, with selectivity index (SI) values of 1.80, 7.88, 3.49, 3.57, and 10.26, respectively, compared to sunitinib (SI = 1.15), suggesting that the compounds possess favorable safety profiles.

Notably, compound **4c** induces cell cycle arrest in HepG2 cells mainly at the G0/G1 phase. Also, it showed a significant increase in the percentages of the apoptotic cells in both early and late apoptosis by 27.75-fold and 76.46-fold, respectively. Additionally, **4c** upregulated the expression of caspase-3 and -9 by 6.51-fold and 2.99-fold, respectively. The wound healing assay further confirmed that **4c** effectively inhibited the migration of cancer cells. Molecular docking study of the active compounds in the VEGFR-2 kinase active site revealed similar binding orientation and interactions to sunitinib. Finally, *in silico* ADME studies showed that the target compounds have promising drug-likeness profiles.

Data availability

The data that support the findings of this study are available as part of the ESI.†

Conflicts of interest

The authors declare that they have no known competing financial interests or personal relationships that could have appeared to influence the work reported in this paper.

Acknowledgements

The authors are grateful to the National Cancer Institute (NCI), Developmental Therapeutic Program (<https://dtp.cancer.gov/>), for screening the *in vitro* anticancer activity for the target compounds over their panel of cell lines. Cell Line cells were obtained from the American Type Culture Collection.

References

- H. Sung, J. Ferlay, R. L. Siegel, M. Laversanne, I. Soerjomataram, A. Jemal and F. Bray, Global Cancer Statistics 2020: GLOBOCAN Estimates of Incidence and Mortality Worldwide for 36 Cancers in 185 Countries, *Ca-Cancer J. Clin.*, 2021, **71**(3), 209–249, DOI: [10.3322/caac.21660](https://doi.org/10.3322/caac.21660).
- F. Bray, M. Laversanne, H. Sung, J. Ferlay, R. L. Siegel, I. Soerjomataram and A. Jemal, Global cancer statistics 2022: GLOBOCAN estimates of incidence and mortality worldwide for 36 cancers in 185 countries, *Ca-Cancer J. Clin.*, 2024, **74**(3), 229–263, DOI: [10.3322/caac.21834](https://doi.org/10.3322/caac.21834).
- R. L. Siegel, T. B. Kratzer, A. N. Giaquinto, H. Sung and A. Jemal, Cancer statistics, 2025, *Ca-Cancer J. Clin.*, 2025, **75**(1), 10–45, DOI: [10.3322/caac.21871](https://doi.org/10.3322/caac.21871).
- I. Soerjomataram and F. Bray, Planning for tomorrow: global cancer incidence and the role of prevention 2020–2070, *Nat. Rev. Clin. Oncol.*, 2021, **18**, 663–672, DOI: [10.1038/s41571-021-00514-z](https://doi.org/10.1038/s41571-021-00514-z).
- J. J. Mao, G. G. Pillai, C. J. Andrade, J. A. Ligibel, P. Basu, L. Cohen, I. A. Khan, K. M. Mustian, R. Puthiyedath, K. S. Dhiman, L. Lao, R. Ghelman, P. Cáceres Guido, G. Lopez, D. F. Gallego-Perez and L. A. Salicrup, Integrative oncology: Addressing the global challenges of cancer prevention and treatment, *Ca-Cancer J. Clin.*, 2022, **72**(2), 144–164, DOI: [10.3322/caac.21706](https://doi.org/10.3322/caac.21706).
- B. S. Chhikara and K. Parang, Global Cancer Statistics 2022: the trends projection analysis, *Chem. Biol. Lett.*, 2023, **10**(1), 451.
- L. Qin, J. L. Bromberg-White and C. N. Qian, in *Adv Cancer Res*, Opportunities and Challenges in Tumor Angiogenesis Research: Back and Forth Between Bench and Bed, Academic Press Inc., 2012, vol. 113, pp. 191–239, DOI: [10.1016/B978-0-12-394280-7.00006-3](https://doi.org/10.1016/B978-0-12-394280-7.00006-3).
- Z. L. Liu, H. H. Chen, L. L. Zheng, L. P. Sun and L. Shi, Angiogenic signaling pathways and anti-angiogenic therapy for cancer, *Signal Transduction Targeted Ther.*, 2023, **8**(1), 198, DOI: [10.1038/s41392-023-01460-1](https://doi.org/10.1038/s41392-023-01460-1).
- J. Majidpoor and K. Mortezaee, Angiogenesis as a hallmark of solid tumors-clinical perspectives, *Cell. Oncol.*, 2021, **44**(4), 715–737, DOI: [10.1007/s13402-021-00602-3](https://doi.org/10.1007/s13402-021-00602-3).
- J. Folkman, Role of angiogenesis in tumor growth and metastasis, *Semin. Oncol.*, 2002, **29**, 15–18, DOI: [10.1053/sonc.2002.37263](https://doi.org/10.1053/sonc.2002.37263).
- R. Lugano, M. Ramachandran and A. Dimberg, Tumor angiogenesis: causes, consequences, challenges and

- opportunities, *Cell. Mol. Life Sci.*, 2020, 77, 1745–1770, DOI: [10.1007/s00018-019-03351-7](#).
- 12 P. Carmeliet, VEGF as a key mediator of angiogenesis in cancer, *Onco Targets Ther*, 2005, 69, 4–10, DOI: [10.1159/000088478](#).
 - 13 X. Wang, A. M. Bove, G. Simone and B. Ma, Molecular Bases of VEGFR-2-Mediated Physiological Function and Pathological Role, *Front. Cell Dev. Biol.*, 2020, 8, 599281, DOI: [10.3389/fcell.2020.599281](#).
 - 14 G. Korpanty, L. A. Sullivan, E. Smyth, D. N. Carney and R. A. Brekken, Molecular and clinical aspects of targeting the VEGF pathway in tumors, *J. Oncol.*, 2010, 2010(1), 652320, DOI: [10.1155/2010/652320](#).
 - 15 A. K. Olsson, A. Dimberg, J. Kreuger and L. Claesson-Welsh, VEGF receptor signalling - In control of vascular function, *Nat. Rev. Mol. Cell Biol.*, 2006, 7(5), 359–371, DOI: [10.1038/nrm1911](#).
 - 16 S. J. Modi and V. M. Kulkarni, Exploration of structural requirements for the inhibition of VEGFR-2 tyrosine kinase: Binding site analysis of type II, 'DFG-out' inhibitors, *J. Biomol. Struct. Dyn.*, 2022, 40(12), 5712–5727, DOI: [10.1080/07391102.2021.1872417](#).
 - 17 Y. Liu and N. S. Gray, Rational design of inhibitors that bind to inactive kinase conformations, *Nat. Chem. Biol.*, 2006, 2, 358–364, DOI: [10.1038/nchembio799](#).
 - 18 K. Sanphanya, S. K. Wattanapitayakul, S. Phowichit, V. V. Fokin and O. Vajragupta, Novel VEGFR-2 kinase inhibitors identified by the back-to-front approach, *Bioorg. Med. Chem. Lett.*, 2013, 23, 2962–2967, DOI: [10.1016/j.bmcl.2013.03.042](#).
 - 19 L. Huang, Z. Huang, Z. Bai, R. Xie, L. Sun and K. Lin, Development and strategies of VEGFR-2/KDR inhibitors, *Future Med. Chem.*, 2012, 4(14), 1839–1852, DOI: [10.4155/fmc.12.121](#).
 - 20 Y. Liu, Y. Li, Y. Wang, C. Lin, D. Zhang, J. Chen, L. Ouyang, F. Wu, J. Zhang and L. Chen, Recent progress on vascular endothelial growth factor receptor inhibitors with dual targeting capabilities for tumor therapy, *J. Hematol. Oncol.*, 2022, 15(1), 89, DOI: [10.1186/s13045-022-01310-7](#).
 - 21 M. S. Elkotamy, M. K. Elgohary, S. T. Al-Rashood, H. Almahli, W. M. Eldehna and H. A. Abdel-Aziz, Novel imidazo[2,1-b]thiazoles and imidazo[1,2-a]pyridines tethered with indolinone motif as VEGFR-2 inhibitors and apoptotic inducers: Design, synthesis and biological evaluations, *Bioorg. Chem.*, 2024, 151, 107644, DOI: [10.1016/j.bioorg.2024.107644](#).
 - 22 H. K. Mahmoud, T. A. Farghaly, H. G. Abdulwahab, N. T. Al-Qurashi and M. R. Shaaban, Novel 2-indolinone thiazole hybrids as sunitinib analogues: Design, synthesis, and potent VEGFR-2 inhibition with potential anti-renal cancer activity, *Eur. J. Med. Chem.*, 2020, 208, 112752, DOI: [10.1016/j.ejmech.2020.112752](#).
 - 23 R. Rana, N. Kumar, H. K. Gulati, A. Sharma, A. Khanna, Pooja, R. Badhwar, M. Dhir, Jyoti, J. V. Singh and P. M. S. Bedi, A comprehensive review on thiazole based conjugates as anti-cancer agents, *J. Mol. Struct.*, 2023, 1292, 136194, DOI: [10.1016/j.molstruc.2023.136194](#).
 - 24 A. F. Kassem, R. H. Althomali, M. M. Anwar and W. I. El-Sofany, Thiazole moiety: A promising scaffold for anticancer drug discovery, *J. Mol. Struct.*, 2024, 1303, 137510, DOI: [10.1016/j.molstruc.2024.137510](#).
 - 25 H. A. Mahdy, H. Elkady, W. E. Elgammal, E. B. Elkaeed, A. A. Alsouk, I. M. Ibrahim, D. Z. Husein, M. A. Elkady, A. M. Metwaly and I. H. Eissa, Design, synthesis, in vitro, and in silico studies of new thiadiazol derivatives as promising VEGFR-2 inhibitors and apoptosis inducers, *J. Mol. Struct.*, 2024, 1316, 139019, DOI: [10.1016/j.molstruc.2024.139019](#).
 - 26 M. Moradi, A. Mousavi, Z. Emamgholipour, J. Giovannini, S. Moghimi, F. Peytam, A. Honarmand, S. Bach and A. Foroumadi, Quinazoline-based VEGFR-2 inhibitors as potential anti-angiogenic agents: A contemporary perspective of SAR and molecular docking studies, *Eur. J. Med. Chem.*, 2023, 259, 115626, DOI: [10.1016/j.ejmech.2023.115626](#).
 - 27 N. A. Alsaif, M. A. Dahab, M. M. Alanazi, A. J. Obaidullah, A. A. Al-Mehizia, M. M. Alanazi, S. Aldawas, H. A. Mahdy and H. Elkady, New quinoxaline derivatives as VEGFR-2 inhibitors with anticancer and apoptotic activity: Design, molecular modeling, and synthesis, *Bioorg. Chem.*, 2021, 110, 104807, DOI: [10.1016/j.bioorg.2021.104807](#).
 - 28 A. G. A. El-Helby, H. Sakr, I. H. Eissa, H. Abulkhair, A. A. Al-Karmalawy and K. El-Adl, Design, synthesis, molecular docking, and anticancer activity of benzoxazole derivatives as VEGFR-2 inhibitors, *Arch. Pharm.*, 2019, 352(10), 1900113, DOI: [10.1002/ardp.201900113](#).
 - 29 M. Hagra, M. A. Saleh, R. R. Ezz Eldin, A. A. Abuelkhir, E. G. Khidr, A. A. El-Husseiny, H. A. El-Mahdy, E. B. Elkaeed and I. H. Eissa, 1,3,4-Oxadiazole-naphthalene hybrids as potential VEGFR-2 inhibitors: design, synthesis, antiproliferative activity, apoptotic effect, and in silico studies, *J. Enzyme Inhib. Med. Chem.*, 2022, 37(1), 386–402, DOI: [10.1080/14756366.2021.2015342](#).
 - 30 I. H. Eissa, H. Elkady, M. Rashed, A. Elwan, M. Hagra, M. A. Dahab, M. S. Taghour, I. M. Ibrahim, D. Z. Husein, E. B. Elkaeed, H. A. Al-ghulikah, A. M. Metwaly and H. A. Mahdy, Discovery of new thiazolidine-2,4-dione derivatives as potential VEGFR-2 inhibitors: In vitro and in silico studies, *Heliyon*, 2024, 10(2), e24005, DOI: [10.1016/j.heliyon.2024.e24005](#).
 - 31 M. Adel and K. A. M. Abouzid, New fluorinated diarylureas linked to pyrrolo[2,3-d]pyrimidine scaffold as VEGFR-2 inhibitors: Molecular docking and biological evaluation, *Bioorg. Chem.*, 2022, 127, 106006, DOI: [10.1016/j.bioorg.2022.106006](#).
 - 32 M. Kashyap, S. Gupta, Y. Bansal and G. Bansal, A critical analysis of design, binding pattern and SAR of benzo-fused heteronuclear compounds as VEGFR-2 inhibitors, *Bioorg. Med. Chem.*, 2024, 115, 117966, DOI: [10.1016/j.bmc.2024.117966](#).
 - 33 A. Thakur, M. Rana, A. Mishra, C. Kaur, C. H. Pan and K. Nepali, Recent advances and future directions on small molecule VEGFR inhibitors in oncological conditions, *Eur. J. Med. Chem.*, 2024, 272, 116472, DOI: [10.1016/j.ejmech.2024.116472](#).

- 34 M. A. Abdelgawad, A. M. Hayallah, S. N. A. Bukhari, A. Musa, M. Elmowafy, H. M. Abdel-Rahman and M. K. Abd El-Gaber, Design, Synthesis, Molecular Modeling, and Anticancer Evaluation of New VEGFR-2 Inhibitors Based on the Indolin-2-One Scaffold, *Pharmaceuticals*, 2022, **15**(11), 1416, DOI: [10.3390/ph15111416](https://doi.org/10.3390/ph15111416).
- 35 S. M. Abou-Seri, A. A. M. Eissa, M. G. M. Behery and F. A. Omar, Synthesis, in vitro anticancer activity and in silico studies of certain isoxazole-based carboxamides, ureates, and hydrazones as potential inhibitors of VEGFR2, *Bioorg. Chem.*, 2021, **116**, 105334, DOI: [10.1016/j.bioorg.2021.105334](https://doi.org/10.1016/j.bioorg.2021.105334).
- 36 S. A. El-Metwally, M. M. Abou-El-Regal, I. H. Eissa, A. B. M. Mehany, H. A. Mahdy, H. Elkady, A. Elwan and E. B. Elkaeed, Discovery of thieno[2,3-d]pyrimidine-based derivatives as potent VEGFR-2 kinase inhibitors and anti-cancer agents, *Bioorg. Chem.*, 2021, **112**, 104947, DOI: [10.1016/j.bioorg.2021.104947](https://doi.org/10.1016/j.bioorg.2021.104947).
- 37 T. Al-Warhi, M. Abualnaja, O. A. Abu Ali, N. M. Alyamani, F. G. Elsaid, A. A. Shati, S. Albogami, E. Fayad, A. H. Abu Almaaty, K. O. Mohamed, W. M. Alamoudi and I. Zaki, Design, Synthesis and Cytotoxicity Screening of New Thiazole Derivatives as Potential Anticancer Agents through VEGFR-2 Inhibition, *Symmetry*, 2022, **14**(9), 1814, DOI: [10.3390/sym14091814](https://doi.org/10.3390/sym14091814).
- 38 E. B. Elkaeed, R. G. Yousef, M. M. Khalifa, A. Ibrahim, A. B. M. Mehany, I. M. M. Gobaara, B. A. Alsouk, W. M. Eldehna, A. M. Metwaly, I. H. Eissa and M. A. El-Zahabi, Discovery of New VEGFR-2 Inhibitors: Design, Synthesis, Anti-Proliferative Evaluation, Docking, and MD Simulation Studies, *Molecules*, 2022, **27**(19), 6203, DOI: [10.3390/molecules27196203](https://doi.org/10.3390/molecules27196203).
- 39 H. M. Alkahtani, M. M. Alanazi, F. S. Aleanizy, F. Y. Alqahtani, A. Alhoshani, F. E. Alanazi, A. A. Almeshizia, A. N. Abdalla, M. G. Alanazi, A. S. El-Azab and A. A. M. Abdel-Aziz, Synthesis, anticancer, apoptosis-inducing activities and EGFR and VEGFR2 assay mechanistic studies of 5,5-diphenylimidazolidine-2,4-dione derivatives: Molecular docking studies, *Saudi Pharm. J.*, 2019, **27**(5), 682–693, DOI: [10.1016/j.jsps.2019.04.003](https://doi.org/10.1016/j.jsps.2019.04.003).
- 40 L. A. Barros Freitas, A. Caroline da Silva Santos, G. de Cássia Silva, F. Nayara do Nascimento Albuquerque, E. D. Silva, C. Alberto de Simone, V. R. Alves Pereira, L. C. Alves, F. A. Brayner, A. C. Lima Leite and P. A. T. de Moraes Gomes, Structural improvement of new thiazolyl-isatin derivatives produces potent and selective trypanocidal and leishmanicidal compounds, *Chem.-Biol. Interact.*, 2021, **345**, 109561, DOI: [10.1016/j.cbi.2021.109561](https://doi.org/10.1016/j.cbi.2021.109561).
- 41 E. M. Othman, E. A. Fayed, E. M. Husseiny and H. S. Abulkhair, Rationale design, synthesis, cytotoxicity evaluation, and in silico mechanistic studies of novel 1,2,3-triazoles with potential anticancer activity, *New J. Chem.*, 2022, **46**(25), 12206–12216, DOI: [10.1039/d2nj02061k](https://doi.org/10.1039/d2nj02061k).
- 42 W. H. Zhao, J. H. Xu, V. K. R. Tangadanchu and C. H. Zhou, Thiazolyl hydrazineylidenyl indolones as unique potential multitargeting broad-spectrum antimicrobial agents, *Eur. J. Med. Chem.*, 2023, **256**, 115452, DOI: [10.1016/j.ejmech.2023.115452](https://doi.org/10.1016/j.ejmech.2023.115452).
- 43 H. Abul-Khair, S. Elmeligie, A. Bayoumi, A. Ghiaty, A. El-Morsy and M. H. Hassan, Synthesis and evaluation of some new (1,2,4) triazolo(4,3-a)quinoxalin-4(5h)-one derivatives as AMPA receptor antagonists, *J. Heterocyclic Chem.*, 2013, **50**, 1202–1208, DOI: [10.1002/jhet.714](https://doi.org/10.1002/jhet.714).
- 44 M. İ. Han, P. Atalay, C. Ü. Tunç, G. Ünal, S. Dayan, Ö. Aydın and G. Küçüküzgel, Design and synthesis of novel (S)-Naproxen hydrazide-hydrazones as potent VEGFR-2 inhibitors and their evaluation in vitro/in vivo breast cancer models, *Bioorg. Med. Chem.*, 2021, **37**, 116097, DOI: [10.1016/j.bmc.2021.116097](https://doi.org/10.1016/j.bmc.2021.116097).
- 45 A. A. Al-Karmalawy, M. A. Zeidan, A. A. Elmaaty, M. Sharaky, A. S. A. Yassen, E. F. Khaleel, W. M. Eldehna and H. F. Ashour, Design and synthesis of new 1,2,3-triazole derivatives as VEGFR-2/telomerase downregulatory candidates endowed with apoptotic potential for cancer treatment, *Bioorg. Chem.*, 2025, **156**, 108159, DOI: [10.1016/j.bioorg.2025.108159](https://doi.org/10.1016/j.bioorg.2025.108159).
- 46 S. El-Kalyoubi, S. S. Elbaramawi, A. G. Eissa, E. Al-Ageeli, Y. H. Hobani, A. A. El-Sharkawy, H. T. Mohamed, A. A. Al-Karmalawy and H. S. Abulkhair, Design and synthesis of novel uracil-linked Schiff bases as dual histone deacetylase type II/topoisomerase type I inhibitors with apoptotic potential, *Future Med. Chem.*, 2023, **15**(11), 937–958, DOI: [10.4155/fmc-2023-0112](https://doi.org/10.4155/fmc-2023-0112).
- 47 M. S. Elkotamy, M. K. Elgohary, S. T. Al-Rashood, H. Almahli, W. M. Eldehna and H. A. Abdel-Aziz, Novel imidazo[2,1-b]thiazoles and imidazo[1,2-a]pyridines tethered with indolinone motif as VEGFR-2 inhibitors and apoptotic inducers: Design, synthesis and biological evaluations, *Bioorg. Chem.*, 2024, **151**, 107644, DOI: [10.1016/j.bioorg.2024.107644](https://doi.org/10.1016/j.bioorg.2024.107644).
- 48 N. M. Saadan, W. U. Ahmed, A. A. Kadi, M. S. Al-Mutairi, R. I. Al-Wabli and A. F. M. M. Rahman, Synthesis and Evaluation of Thiazolyl-indole-2-carboxamide Derivatives as Potent Multitarget Anticancer Agents, *ACS Omega*, 2024, **9**(40), 41944–41967, DOI: [10.1021/acsomega.4c06889](https://doi.org/10.1021/acsomega.4c06889).
- 49 M. A. Lopes-Ortiz, M. R. Panice, E. Borges de Melo, J. P. Ataíde Martins, V. P. Baldin, C. T. Agostinho Pires, K. R. Caleffi-Ferracioli, V. L. Dias Siqueira, R. Bertin de Lima Scodro, M. H. Sarragiotto and R. F. Cardoso, Synthesis and anti-Mycobacterium tuberculosis activity of imide- β -carboline and carbomethoxy- β -carboline derivatives, *Eur. J. Med. Chem.*, 2020, **187**, 111935, DOI: [10.1016/j.ejmech.2019.111935](https://doi.org/10.1016/j.ejmech.2019.111935).
- 50 L. B. Salum, A. Mascarello, R. R. Canevarolo, W. F. Alteí, A. B. A. Laranjeira, P. D. Neuenfeldt, T. R. Stumpf, L. D. Chiaradia-Delatorre, L. L. Vollmer, H. N. Daghestani, C. P. De Souza Melo, A. B. Silveira, P. C. Leal, M. J. S. Frederico, L. F. Do Nascimento, A. R. S. Santos, A. D. Andricopulo, B. W. Day, R. A. Yunes, A. Vogt, J. A. Yunes and R. J. Nunes, N-(1'-naphthyl)-3,4,5-trimethoxybenzohydrazide as microtubule destabilizer: Synthesis, cytotoxicity, inhibition of cell migration and in vivo activity against acute lymphoblastic leukemia, *Eur. J. Med. Chem.*, 2015, **96**, 504–518, DOI: [10.1016/j.ejmech.2015.02.041](https://doi.org/10.1016/j.ejmech.2015.02.041).
- 51 H. S. Abulkhair, S. Elmeligie, A. Ghiaty, A. El-Morsy, A. H. Bayoumi, H. E. A. Ahmed, K. El-Adl, M. F. Zayed, M. H.

- Hassan, E. N. Akl and M. S. El-Zoghbi, In vivo- and in silico-driven identification of novel synthetic quinoxalines as anticonvulsants and AMPA inhibitors, *Arch. Pharm.*, 2021, **354**(5), 2000449, DOI: [10.1002/ardp.202000449](https://doi.org/10.1002/ardp.202000449).
- 52 M. S. Abusaif, A. Ragab, E. A. Fayed, Y. A. Ammar, A. M. H. Gowifel, S. O. Hassanin, G. E. Ahmed and N. A. Gohar, Exploring a novel thiazole derivatives hybrid with fluorinated-indenoquinoxaline as dual inhibitors targeting VEGFR2/AKT and apoptosis inducers against hepatocellular carcinoma with docking simulation, *Bioorg. Chem.*, 2025, **154**, 108023, DOI: [10.1016/j.bioorg.2024.108023](https://doi.org/10.1016/j.bioorg.2024.108023).
- 53 U. Acar Çevik, I. Celik, Ş. Görgülü, Z. D. Şahin Inan, H. E. Bostancı, Y. Özkay and Z. A. Kaplacıklı, New benzimidazole-oxadiazole derivatives as potent VEGFR-2 inhibitors: Synthesis, anticancer evaluation, and docking study, *Drug Dev. Res.*, 2024, **85**(4), e22218, DOI: [10.1002/ddr.22218](https://doi.org/10.1002/ddr.22218).
- 54 A. Monks, D. Scudiero, P. Skehan, R. Shoemaker, K. Paull, D. Vistica, C. Hose, J. Langley, P. Cronise, A. Vaigro-Wolff, M. Gray-Goodrich, H. Campbell, J. Mayo and M. Boyd, Feasibility of a High-Flux Anticancer Drug Screen Using a Diverse Panel of Cultured Human Tumor Cell Lines, *J. Natl. Cancer Inst.*, 1991, **83**(11), 757–766, DOI: [10.1093/jnci/83.11.757](https://doi.org/10.1093/jnci/83.11.757).
- 55 M. R. Boyd and K. D. Padl, Some Practical Considerations and Applications of the National Cancer Institute In Vitro Anticancer Drug Discovery Screen, *Drug Dev. Res.*, 1995, **34**, 91–109.
- 56 E. M. Othman, E. A. Fayed, E. M. Husseiny and H. S. Abulkhair, The effect of novel synthetic semicarbazone- and thiosemicarbazone-linked 1,2,3-triazoles on the apoptotic markers, VEGFR-2, and cell cycle of myeloid leukemia, *Bioorg. Chem.*, 2022, **127**, 105968, DOI: [10.1016/j.bioorg.2022.105968](https://doi.org/10.1016/j.bioorg.2022.105968).
- 57 S. Peng, Y. Wang, H. Peng, D. Chen, S. Shen, B. Peng, M. Chen, R. Lencioni and M. Kuang, Autocrine vascular endothelial growth factor signaling promotes cell proliferation and modulates sorafenib treatment efficacy in hepatocellular carcinoma, *Hepatology*, 2014, **60**(4), 1264–1277, DOI: [10.1002/hep.27236](https://doi.org/10.1002/hep.27236).
- 58 Q. Xiang, W. Chen, M. Ren, J. Wang, H. Zhang, D. Y. B. Deng, L. Zhang, C. Shang and Y. Chen, Cabozantinib suppresses tumor growth and metastasis in hepatocellular carcinoma by a dual blockade of VEGFR2 and MET, *Clin. Cancer Res.*, 2014, **20**(11), 2959–2970, DOI: [10.1158/1078-0432.CCR-13-2620](https://doi.org/10.1158/1078-0432.CCR-13-2620).
- 59 G. M. Cohen, Caspases : the executioners of apoptosis, *Biochem. J.*, 1997, **326**, 1–16, DOI: [10.1042/bj3260001](https://doi.org/10.1042/bj3260001).
- 60 S. H. Mackenzie and A. C. Clark, Targeting Cell Death in Tumors by Activating Caspases, *Curr. Cancer Drug Targets*, 2008, **8**(2), 98–109, DOI: [10.2174/156800908783769391](https://doi.org/10.2174/156800908783769391).
- 61 L. Lamalice, F. Le Boeuf and J. Huot, Endothelial cell migration during angiogenesis, *Circ. Res.*, 2007, **100**(6), 782–794, DOI: [10.1161/01.RES.0000259593.07661.1e](https://doi.org/10.1161/01.RES.0000259593.07661.1e).
- 62 M. McTigue, B. W. Murray, J. H. Chen, Y. L. Deng, J. Solowiej and R. S. Kania, Molecular conformations, interactions, and properties associated with drug efficiency and clinical performance among VEGFR TK inhibitors, *Proc. Natl. Acad. Sci. U. S. A.*, 2012, **109**(45), 18281–18289, DOI: [10.1073/pnas.1207759109](https://doi.org/10.1073/pnas.1207759109).
- 63 M. P. Gleeson, A. Hersey, D. Montanari and J. Overington, Probing the links between in vitro potency, ADMET and physicochemical parameters, *Nat. Rev. Drug Discovery*, 2011, **10**(3), 197–208, DOI: [10.1038/nrd3367](https://doi.org/10.1038/nrd3367).
- 64 A. Daina, O. Michielin and V. Zoete, SwissADME: A free web tool to evaluate pharmacokinetics, drug-likeness and medicinal chemistry friendliness of small molecules, *Sci. Rep.*, 2017, **7**, 42717, DOI: [10.1038/srep42717](https://doi.org/10.1038/srep42717).
- 65 D. M. Mamand, D. M. Aziz, H. M. Qadr and A. H. Awla, Quantum Computational Chemistry and Optoelectronic Properties of a New Synthesis Organic Compound, *J. Mex. Chem. Soc.*, 2024, **68**(3), 513–526, DOI: [10.29356/jmcs.v68i3.1946](https://doi.org/10.29356/jmcs.v68i3.1946).
- 66 D. Pegu, J. Deb, C. Van Alsenoy and U. Sarkar, Theoretical investigation of electronic, vibrational, and nonlinear optical properties of 4-fluoro-4-hydroxybenzophenone, *Spectrosc. Lett.*, 2017, **50**(4), 232–243, DOI: [10.1080/00387010.2017.1308381](https://doi.org/10.1080/00387010.2017.1308381).
- 67 I. H. Eissa, M. M. Khalifa, E. B. Elkaeed, E. E. Hafez, A. A. Alsouk and A. M. Metwaly, In silico exploration of potential natural inhibitors against sars-cov-2 nsp10, *Molecules*, 2021, **26**(20), 6151, DOI: [10.3390/molecules26206151](https://doi.org/10.3390/molecules26206151).
- 68 J. C. Rodríguez, R. A. Maldonado, G. Ramírez-García, E. Díaz Cervantes and F. N. de la Cruz, Microwave-assisted synthesis and luminescent activity of imidazo[1,2-a]pyridine derivatives, *J. Heterocyclic Chem.*, 2020, **57**(5), 2279–2287, DOI: [10.1002/jhet.3950](https://doi.org/10.1002/jhet.3950).
- 69 P. O. Venkataramana Reddy, S. Mishra, M. P. Tantak, K. Nikhil, R. Sadana, K. Shah and D. Kumar, Design, synthesis and in vitro cytotoxicity studies of novel β -carbolinium bromides, *Bioorg. Med. Chem. Lett.*, 2017, **27**(6), 1379–1384, DOI: [10.1016/j.bmcl.2017.02.010](https://doi.org/10.1016/j.bmcl.2017.02.010).